AD-A105 811 MASSACHUSETTS INST OF TECH LEXINGTON LINCOLN LAB F/G 20/5
AMORPHOUS-CRYSTALLINE BOUNDARY DYNAMICS IN LASER CRYSTALLIZATIO--ETC(U)
AUG 81 H J ZEIGER, J C FAN, B J PALM F19628-80-C-0002
UNCLASSIFIED TR-558 ESD-TR-81-85 NL

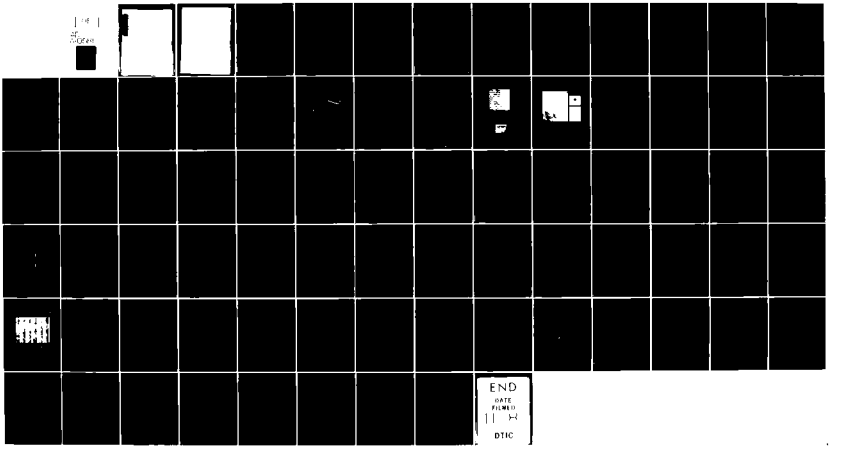

MASSACHUSETTS INSTITUTE OF TECHNOLOGY
LINCOLN LABORATORY

AMORPHOUS-CRYSTALLINE BOUNDARY DYNAMICS IN LASER CRYSTALLIZATION

H.J. ZEIGER
J.C.C. FAN
B.J. PALM
R.L. CHAPMAN
R.P. GALE
Group 83

TECHNICAL REPORT 558

25 AUGUST 1981

LEXINGTON MASSACHUSETTS

Abstract

Two theoretical descriptions have been developed for the phase boundary dynamics during crystallization of amorphous films by scanning with the slit image of a cw laser or of any cw energy beam. The first reduces the problem to the solution of a one-dimensional integral equation, which allows a choice of initial conditions. Depending on the background temperature, numerical solutions yield either periodic or runaway motion of the amorphous-crystalline (a-c) boundary, as observed in experiments on scanned laser crystallization of thin films of a-Ge on fused-silica substrates. The calculations give a semi-quantitative fit to the experimental results for the spatial periodicity observed in the crystallized films as a function of background temperature. Profiles of film temperature as a function of distance from the laser image at successive times have been computed for both the periodic and runaway cases. The model qualitatively explains many of the effects observed during scanned cw laser crystallization, including periodic fluctuations in light emission. The second theoretical description is a more exact two-dimensional treatment, applicable only to cases of steady-state motion of the a-c boundary, which rigorously handles heat flow into the substrate. This treatment has been used to calculate the boundary velocity during steady-state runaway. The dependence of this velocity on background temperature and on film and substrate thermal properties and thickness has been determined. At the minimum background temperature required for runaway the calculated value of the steady-state velocity is ~ 140 cm/sec for the case of a Ge film 0.3 μm

thick on a fused-silica substrate 1 mm thick. Experimental values lie in the range 100-300 cm/sec. A class of laser-controlled steady-state solutions has been obtained for which the boundary velocity is equal to the laser scanning velocity but lower than the boundary velocity for uncontrolled runaway. The existence of these solutions suggests the possibility of preparing single-crystal semiconductor sheets by scanning amorphous films in a manner that achieves uniform, laser-controlled motion of the a-c boundary rather than either periodic or runaway motion.

CONTENTS

ILLUSTRATIONS

I. Introduction

The study of the transformation of semiconductor films from the amorphous to the crystalline state has become a matter of great interest in the last few years. The time dependence of the transformation has been investigated as a function of film temperature for Ge[1] and Si,[2] and the latent heat of transformation and transformation temperature has been measured for Ge,[3,4] Si,[4] and Ge-Si alloys.[4] The so-called "explosive" transformation of semiconductor films has been reported by a number of workers,[5] and the velocity of the transformation has been measured.[6]

We have recently reported the observation of a number of unusual phenomena during a study of the laser crystallization of amorphous Ge films.[7] These phenomena included the formation of periodic structural features, pulsations of film temperature during laser scanning, and runaway crystallization of the entire film following momentary contact with the laser image. To provide a qualitative description of the laser-crystallization process, we presented a one-dimensional integral equation description of the amorphous-crystalline (a-c) phase boundary motion,[8] which takes into account the latent heat emitted during the a-c transformation. Numerical solution of the integral equation provides considerable insight into the dynamics of the a-c boundary. The results were used to obtain a semiquantitative fit of the temperature dependence of the structural periodicity observed in crystallization of amorphous Ge films on fused silica substrates.

In this report we present a somewhat improved version of the one-dimensional integral equation description of laser crystallization which takes account of the loss of heat to the film substrate by introducing into the equation an ad-hoc exponential time dependent damping factor. The results obtained for the motion of the a-c boundary are qualitatively very similar to those obtained earlier.[8] The solution of the integral equation is used to obtain series of plots of temperature as a function of lateral position in the film at fixed times after the onset of the crystallization process. These plots provide an understanding of the temperature pulsations during the formation of periodic structures in film morphology, as well as a vivid picture of the onset of a-c phase boundary runaway. The general features of the model are strongly supported by our recent experimental study of a-c boundary dynamics during laser crystallization.[9]

The one-dimensional integral equation solutions provide an approximate description of transient as well as steady-state behavior of the a-c phase boundary motion. On the other hand, we have obtained a class of less approximate two-dimensional solutions which are stationary in a frame of reference moving with the a-c phase bounary. It is far more complicated to try to obtain transient solutions of the two-dimensional problem. The stationary solutions are exact if the temperature dependence of film and substrate properties as well as differences in amorphous and crystalline properties are neglected. The solutions allow a calculation of the a-c runaway boundary velocity, as well as the velocity of the boundary when the

laser controls its motion. The runaway velocities calculated are in reasonable agreement with observation.

In Section II of this paper we present the transient and periodic steady-state solutions of the one-dimensional integral equation description of laser crystallization. The model results are compared to experimental results for laser crystallization of a-Ge. In Section III we obtain and compare the steady state runaway solutions of the integral equation approximation and the two dimensional model. In section IV we consider steady state laser-guided solutions obtained from the integral equation approximation and the exact model. In Section V the results obtained and the possibility of achieving steady state laser-guided a-c boundary motion are discussed. The numerical solution of the integral equation is discussed in Appendix A, and the stationary solution of the exact two-dimensional problem is derived in Appendix B.

II. Transient and Periodic Solutions of the Integral Equation

A. Derivation of the Integral Equation

When the temperature of an amorphous semiconductor film is raised, tranformation to the stable crystalline form takes place at a rate that increases exponentially with temperature,[1,2] so that over a narrow temperature interval at a temperature $\sim T_c$ the ratio of the time taken for a laser scan changes from $>>1$ to $<<1$. We therefore argue that a reasonable description of the tranformation is given by assuming that it occurs when the amorphous film reaches a critical temperature T_c. Support for this point of view comes from

the observation of a rather sharply defined transformation temperature in latent heat measurements.[4] It has been suggested[10] that the transformation may in fact correspond to the change from the amorphous to the liquid state, followed by a transformation to the crystalline state. In this case the existence of a well defined transition temperature T_c is expected. The assumption of a transformation at a constant temperature T_c should be a reasonable approximation in either case, and is justified by the good description of experiment that results. The modification of this assumption, and the detailed nature of the transformation are considered further in the discussion of Sec. V.

We assume that the temperature dependence of the film properties and the difference in these properties between the amorphous and crystalline states can be neglected. This is an acceptable approximation at temperatures in the range of the amorphous-crystalline transformation ($\sim$ 500-700°C for Ge). With these simplifying assumptions, an integral equation formalism[11] can be used to describe the motion of the phase boundary. The geometry assumed for the laser crystallization calculation is shown schematically in Fig. 1. The semiconductor film, which is deposited on a thick substrate, is of infinite extent in the y and z directions and so thin that its temperature is constant in the x direction. The laser slit image is of infinite length in the z direction and moves at a velocity v in the positive y direction. At time t = 0, the phase boundary is located at y_0, with the crystalline phase to the left ($y < y_0$) and the untransformed amorphous phase to the right ($y > y_0$). The

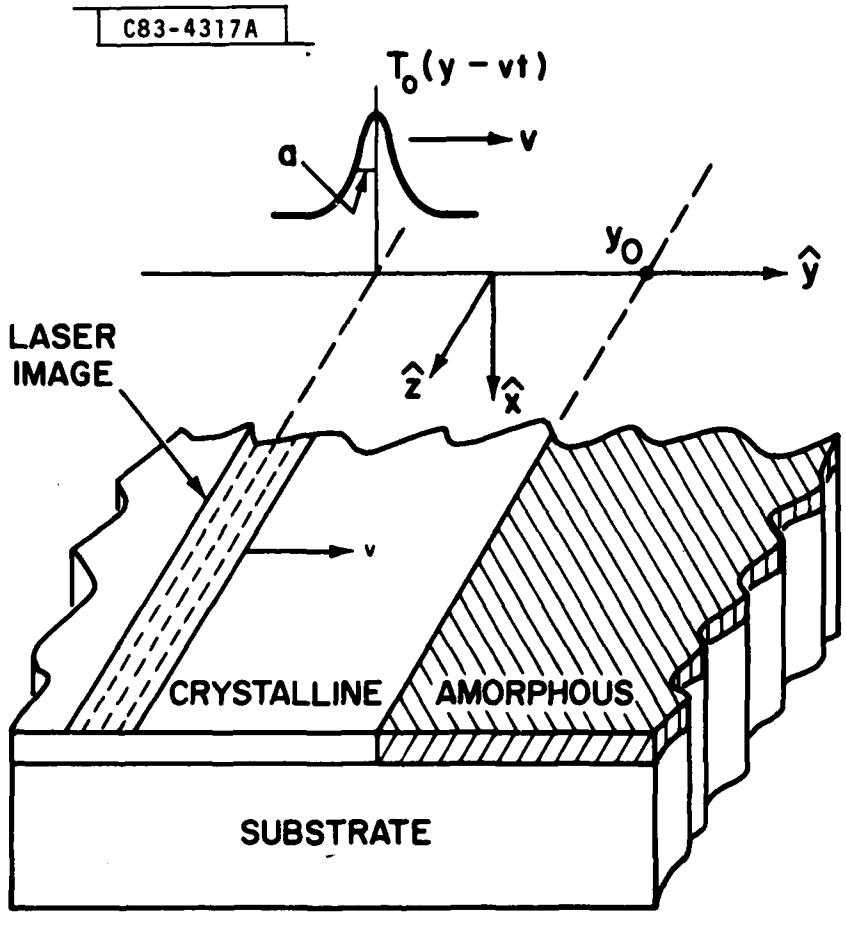

Fig. 1. Schematic representation of laser crystallization experiment.

laser image carries with it a steady state temperature profile T_0 (y-vt). At t = 0, the temperature at the phase boundary reaches T_c and the boundary begins to move irreversibly toward the right, with heat being liberated at a rate per boundary unit cross sectional area of $fL\rho\dot{Y}(t)$, where L is the latent heat of a-c transformation of the semiconductor, ρ is the semiconductor density, Y(t) is the position of the boundary at time t, and we have included a factor f which is less than 1 and accounts in an approximate way for the loss of a fraction (1-f) of the latent heat to the substrate as it is liberated. In the present version, we will also include an exponential damping factor γ to represent the eventual diffusion into the substrate of the fraction f of the heat propagating in the film. We shall see that f and γ, which are introduced as <u>ad hoc</u> parameters in the one-dimensional integral equation, have their counterparts in the two dimensional steady state model (Sec. IIIB), where they are determined in the course of the calculation, leaving no adjustable parameters. The effect of strain and other mechanical forces is not explicitly included, although L could include a contribution due to strain. Then the temperature T(y,t) at any point y along the film at time t is given by the one-dimensional integral relation[11]

$$T(y,t) = T_0\,(y-vt) + \tag{1}$$

$$\frac{fL}{C}\int_0^t \dot{Y}(t')\left[\exp\{-\gamma\,[t-t']\}\right]\left[\exp\left\{\frac{-[y-Y(t')]^2}{4\kappa[t-t']}\right\}\right][4\pi\kappa]^{-1/2}\,[t-t']^{-1/2}\,dt'$$

where C is the specific heat of the film, $\kappa = K/C\rho$ defines its thermal

diffusivity, K is its thermal conductivity, and γ is a phenomenological damping factor.

Equation (1) has a simple physical interpretation. It states that the temperature at a point y at time t is a superposition of the contribution due to the moving laser, T_0 (y-vt), and the sum of contributions due to sources of heat $fL\rho\dot{Y}(t')dt'$, emitted at positions $Y(t')$ at earlier times t'. The source function or Green's function

$$\left[\exp\left\{\frac{-[y - Y(t')]^2}{4\kappa[t - t']}\right\}\right] \quad [4\pi\kappa]^{-1/2} \quad [t-t']^{-1/2}$$

describes the one-dimensional diffusion of heat away from the source, and the factor $\exp\left\{-\gamma[t-t']\right\}$ represents the decay of heat out of the film and into the substrate or atmosphere.

An integral equation for Y(t) can be obtained by using the condition that the temperaure at the phase boundary is T_c, or

$$T\,[Y(t),t] = T_c \quad . \tag{2}$$

For purposes of calculation, it is convenient to rewrite Eq. (2) in the frame of reference moving with the laser image. We introduce the position variable $u(t) = y(t) - vt$, where u(t) is measured from the center of the laser image as origin. The temperature $T_0(u)$ is modeled in the form $T_0(u) = T_b + \Delta T_\ell \exp[-(u/a)^2]$, where T_b is a uniform, time-independent background temperature and the temperature contribution due to the laser is described by a Gaussian of width a and magnitude ΔT_ℓ. Finally, introducing a unit of length d for

normalization purposes and normalizing quantities, we can write the integral equation for the motion of the phase boundary as

$$1 = \alpha \exp\left\{-\frac{[S(\tau)]^2}{b^2}\right\} + \eta \int_0^{\tau} \{[\dot{S}(\tau') + V]/(\tau-\tau')^{1/2}\} \times \left[\exp\{-\Gamma(\tau-\tau')\}\right]\left[\exp\{-[S(\tau)-S(\tau') + V(\tau-\tau')]^2 / (\tau-\tau')\}\right] d\tau' \quad (3)$$

where $\alpha = \Delta T_{\ell}/(T_c-T_b)$, (4a)

$$\eta = f\eta', \ \eta' = L/C\pi^{1/2}(T_c-T_b), \quad (4b)$$

$\tau \equiv 4\kappa t/d^2$, $V \equiv dv/4\kappa$, $S \equiv U/d$, $\dot{S}(\tau') \equiv [dS(\tau')/d\tau']$, $\Gamma = (d^2/4\kappa)\gamma$, $b = a/d$, and U is the position of the phase boundary measured from the center of the laser image. For the discussion of this section, it is convenient to choose $d = a$, so that $b = 1$.

Equation (3) is not in itself sufficient to give physically acceptable solutions for the motion of the phase boundary, since it allows negative values of $[\dot{S}(\tau') + V]$, which imply the unphysical motion of the phase boundary back toward the laser image, with the reconversion of crystalline material to the amorphous state, accompanied by the reabsorption of latent heat. To constrain Eq. (3) to physically acceptable solutions, we require that when the numerical solution of Eq. (3) yields $[\dot{S}(\tau') + V] < 0$, this quantity is to be set equal to zero, with the phase boundary remaining stationary.

Equation (3) has been solved numerically (see appendix A) to obtain S as a function of τ for representative values of α, η, V, and Γ, with the boundary conditions that $\dot{S}(\tau) = 0$ at $\tau = 0$ and that S(0) is given by $1 = \alpha \exp\{-[S(0)]^2\}$. The values of the parameters have been chosen for convenience in numerical solution of Eq. (3) rather than an optimal fit to experimental conditions. Figure 2 shows plots of S vs τ for V = 0.3, Γ = 30 and three increasing values of η, with α increasing in proportion to η (which corresponds, from Eqs. (4a) and (4b), to increasing T_b toward T_c while holding ΔT_ℓ fixed.) For each value of η, S initially increases rapidly because the latent heat liberated by the phase transformation raises the temperature ahead of the boundary, accelerating its forward motion. As the boundary moves away from the laser image, the contribution of the laser to the temperature ahead of the boundary decreases rapidly. For η = 0.3, the boundary motion soon decelerates, and the boundary comes to rest, remaining fixed for a time interval during which its temperature begins to drop rapidly below T_c and S decreases with velocity $\dot{S} = -V$. With the approach of the laser image the boundary temperature gradually increases to T_c, the boundary once more moves forward, and S again increases. This cycle is repeated indefinitely, resulting in the oscillations in S seen for η = 0.3 in Fig. 2. The inset in Fig. 2 shows the result of an experiment[9] which measures the infrared light transmitted through a thin film of Ge as the a-c boundary moves in a cw laser crystallization experiment. Since the transmission of crystalline Ge is much greater than that of amorphous Ge, the changes in transmitted light signal

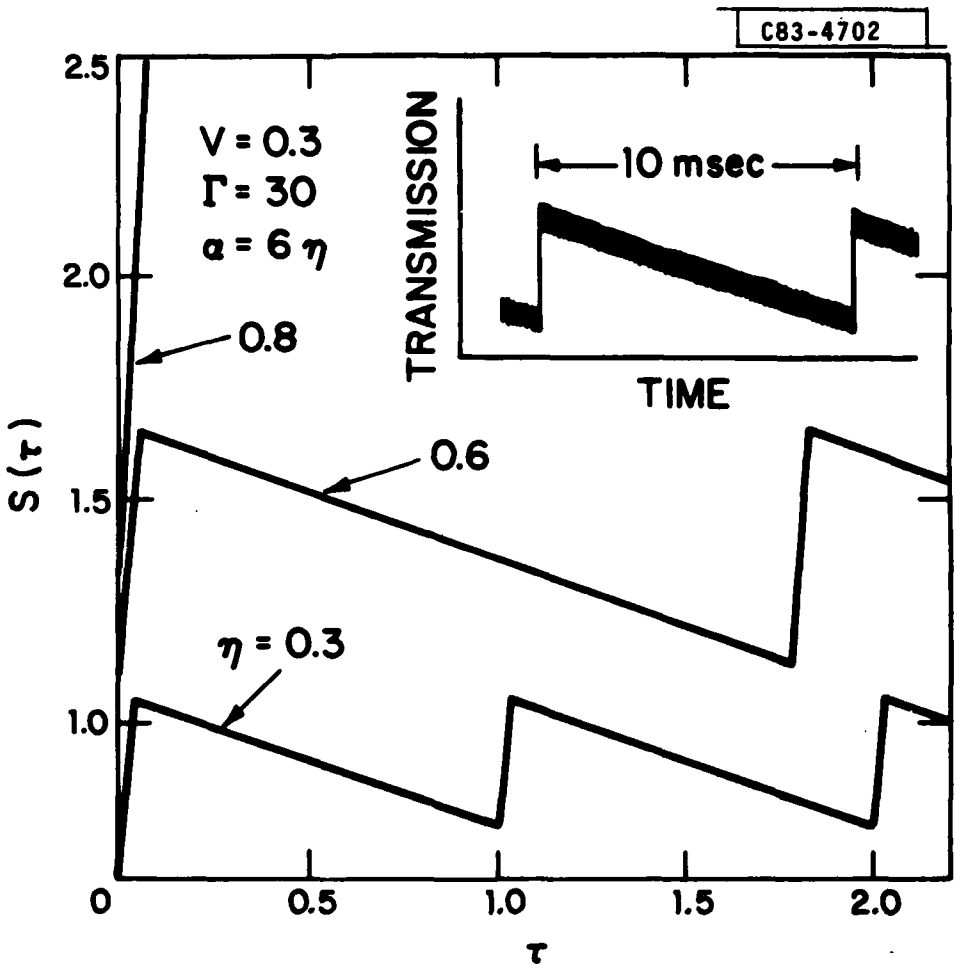

Fig. 2. Normalized position of a-c phase boundary, $S(\tau)$, as a function of normalized time, τ, given by solutions of Eq. (3) for three different values of η. The inset shows the result of an experiment in which change of transmission is proportional to $S(\tau)$.

with time are proportional to the a-c boundary position with time. The similarity between the oscillations observed in the experiment and those shown in the curve for $\eta = 0.3$ is evident.

When η is increased by increasing T_b, less heat is required to raise the temperature of the film to T_c ahead of the laser image, and the phase boundary moves farther beyond the laser before it decelerates and comes to rest. This trend is illustrated by the calculated curve for $\eta = 0.6$ in Fig. 2 and leads to motion with a longer period. When η becomes large enough, the heat liberated during crystallization is sufficient to sustain the transformation, causing the boundary to "run away" from the laser image. This situation, which is illustrated by the curve for $\eta = 0.8$ in Fig. 2, accounts for the observation that for high enough background temperature the entire film is crystallized following momentary contact with the laser image.

In addition to explaining runaway crystallization, the proposed model can also explain our other qualitative observations on laser crystallization. The model does not directly predict observable structural changes in the laser-treated films. However, different regions of such films can be expected to differ in microstructure depending on their rates of transformation and therefore on their thermal history. This suggests that the periodic structural features observed on laser-crystallized films (see Figs. 3 and 4) can be attributed to oscillations in S like those implied by the curves for $\eta = 0.3$ and 0.6 in Fig. 2. Furthermore, for sufficiently high values of η these oscillations produce large fluctuations in the rate of heat liberation

and therefore in temperature. This can explain the periodic fluctuations in light emission observed during some laser crystallization experiments (see Sec. II C).

B. Comparison with Experiment

In order to carry out a semi-quantitative test of the model, we have measured the spatial period of the structural features of laser-crystallized Ge films as a function of T_b.[7] Experiments were performed on amorphous films 0.3 μm thick, deposited on fused silica substrates and scanned at v = 0.5 cm/sec with a slit image of a cw Nd:YAG laser. Initially, a film at room temperature was irradiated at a laser power level just high enough to produce crystallization, which yielded structure in the transformed film with a spatial period of ~ 50 μm. In the following experiments each film was heated to a successively higher value of T_b, the laser scanned at the same power level, and the spacing measured after crystallization. This procedure was continued until T_b approached the value resulting in runaway.

The periodic features obtained by crystallization of a film with T_b of room temperature are shown in Fig. 3, an optical transmission micrograph. These features are shown at higher magnification by the left side of Fig. 4, which is a bright-field micrograph obtained by transmission electron microscopy (TEM) using 125 keV electrons. Each feature consists of four different regions: first a narrow amorphous region, then a region containing a mixture of amorphous material and fine grains, next a broad region of fine grains, and finally another broad region of much larger, elongated

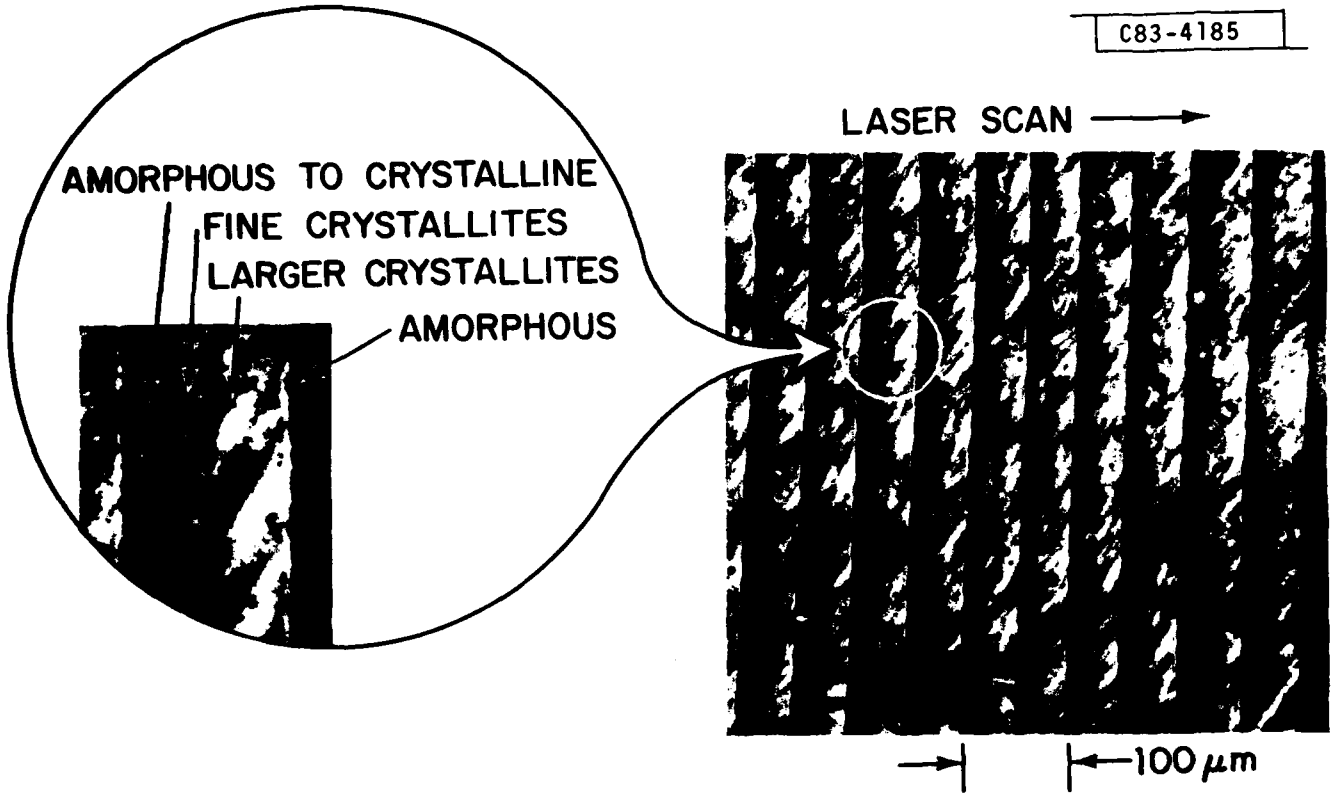

Fig. 3. Optical transmission micrograph of a laser-crystallized Ge film showing periodic structural features. Inset is expanded view illustrating four different microstructure regions.

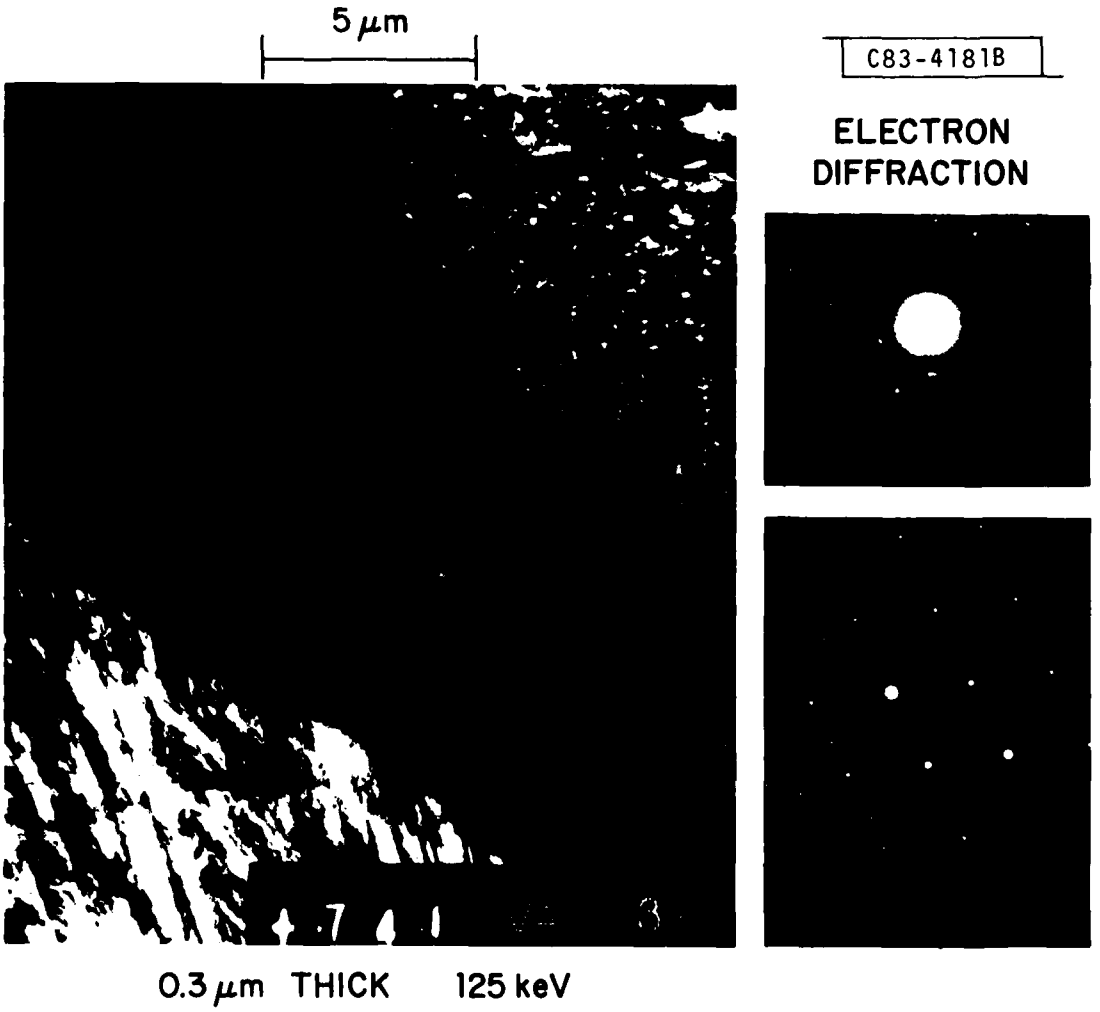

Fig. 4. Left: Bright-field transmission-electron micrograph of a laser-crystallized Ge film, illustrating four different microstructure regions. Right: Transmission-electron diffraction patterns for fine-grained and large-grained regions (upper and lower, respectively).

crystallites aligned parallel to each other. The fine-grained region yields transmission electron diffraction patterns like the one shown at the upper right of Fig. 4, with the rings typical of polycrystalline material. The large crystallites of the final region are clearly visible as ribbon-like structures in the lower left corner of the TEM micrograph, and yield characteristic single-crystal transmission electron diffraction patterns, as illustrated at the lower right of Fig. 4. It should be emphasized that these large aligned crystallites are produced without the presence of a relief structure in the amorphous silica substrate.[12] The nature of the crystalline structure within each period is discussed further in Sec. V.

To use the model to calculate the spatial period in the film, we assume that this period is equal to the distance ΔY traversed by the a-c phase boundary during each of its successive jumps, from the point where crystallization is initiated by the approaching laser to the point where the boundary comes to rest ahead of the laser. This distance is just equal to $(aV\Delta\tau)$, where V is the normalized laser scanning velocity and $\Delta\tau$ is the normalized time interval between the beginnings of two successive jumps, i.e., the period of the oscillations in S illustrated by the curves for $\eta = 0.3$ and 0.6 in Fig. 2.

To obtain a relationship between ΔY and T_b, we first used Eq. (3) to calculate $V\Delta\tau$ as a function of η for representative values of α, V, and Γ. Because of the introduction of the new damping parameter Γ, the results obtained are numerically somewhat different from those reported earlier,[7,8]

but are qualitatively unchanged. The calculated curve for $\alpha = 6\ \eta$ (corresponding to fixed ΔT_ℓ), $V = 0.3$, and $\Gamma = 30$ is shown in Fig. 5. With increasing η, $\Delta\tau$ and therefore $V\Delta\tau$ increase rapidly, leading to boundary runaway by $\eta \approx 0.69$. For a given value of η, $V\Delta\tau$ is found to be quite insensitive to either α or V, showing that the boundary jump distance is determined primarily by the properties of the film and by T_b, and does not depend strongly on either the power or velocity of the laser.

In order to compare theory with experiment, the curve of $V\Delta\tau$ vs η shown in Fig. 5 was used to obtain curves relating the ratios $\Delta Y/\Delta Y_o$ and T_b/T_c, where ΔY_o is the spatial period in the film (i.e., the boundary jump distance) for T_b of room temperature. To calculate these curves, Eq. (4b) was rewritten in the lumped-parameter form $\eta = \eta_o/(1-T_b/T_c)$, where $\eta_o \equiv fL/\pi^{1/2}CT_c$. If T_b and T_c are expressed in °C, room temperaure is much less than T_c, so that $\eta_o \approx \eta$ at room temperature, and ΔY_o corresponds to η_o. Curves of $\Delta Y/\Delta Y_o$ vs $T_b/T_c = 1-\eta_o/\eta$ were calculated by adopting pairs of numerical values of η_o and T_c, then compared with the experimental points (for each point, the adopted value of T_c was used to determine T_b/T_c). A reasonable overall fit has been obtained, as shown in Fig.6, for $\eta_o \approx 0.22$ and $T_c \approx 680$°C. The abrupt increase in $\Delta Y/\Delta Y_o$ when T_b/T_c exceeds about 0.6 is associated with the approach of T_b to the value T_r above which laser irradiation results in boundary runaway. From Fig. 6, using $T_c \sim 680$°C, $T_r \sim [0.7\ T_c] = 500$°C. It is interesting to note that Bagley and Chen[10] predict a transformation of a-Ge to the liquid state at a temperature of 696°C, well below the crystalline-to-liquid

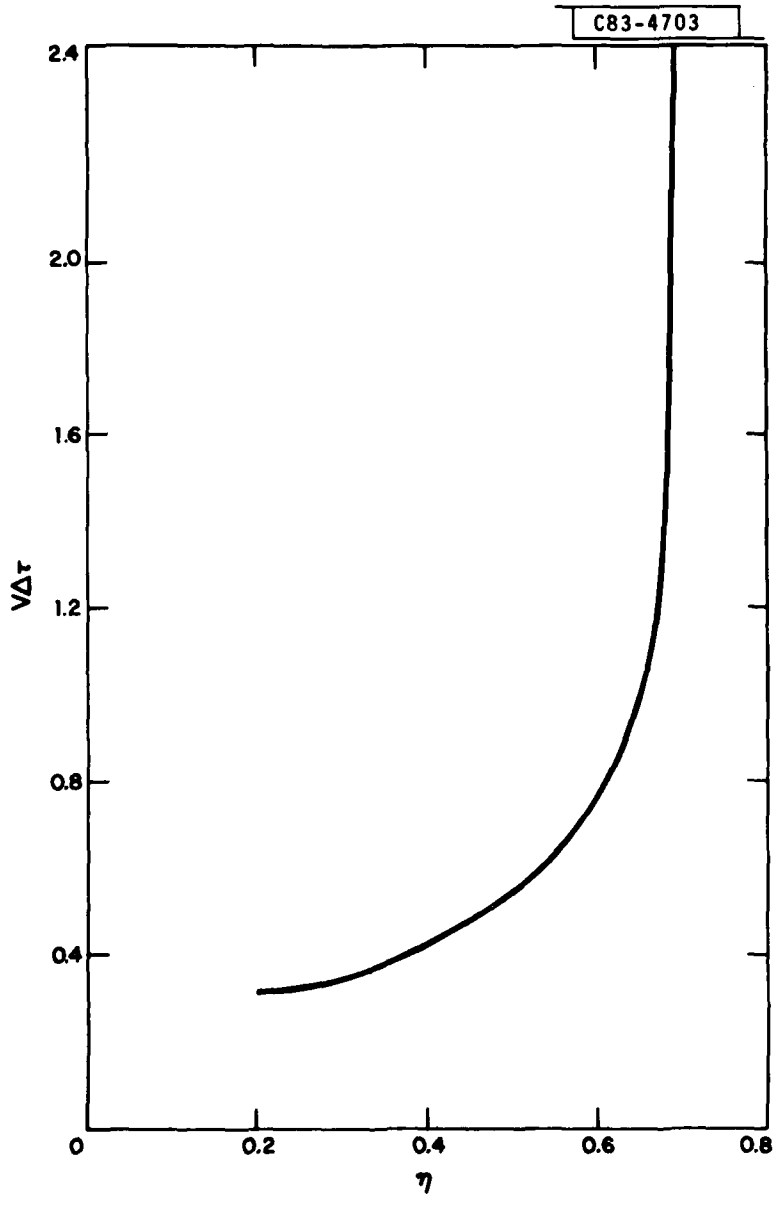

Fig. 5. $V\Delta\tau$ vs η from solutions of Eq. (3).

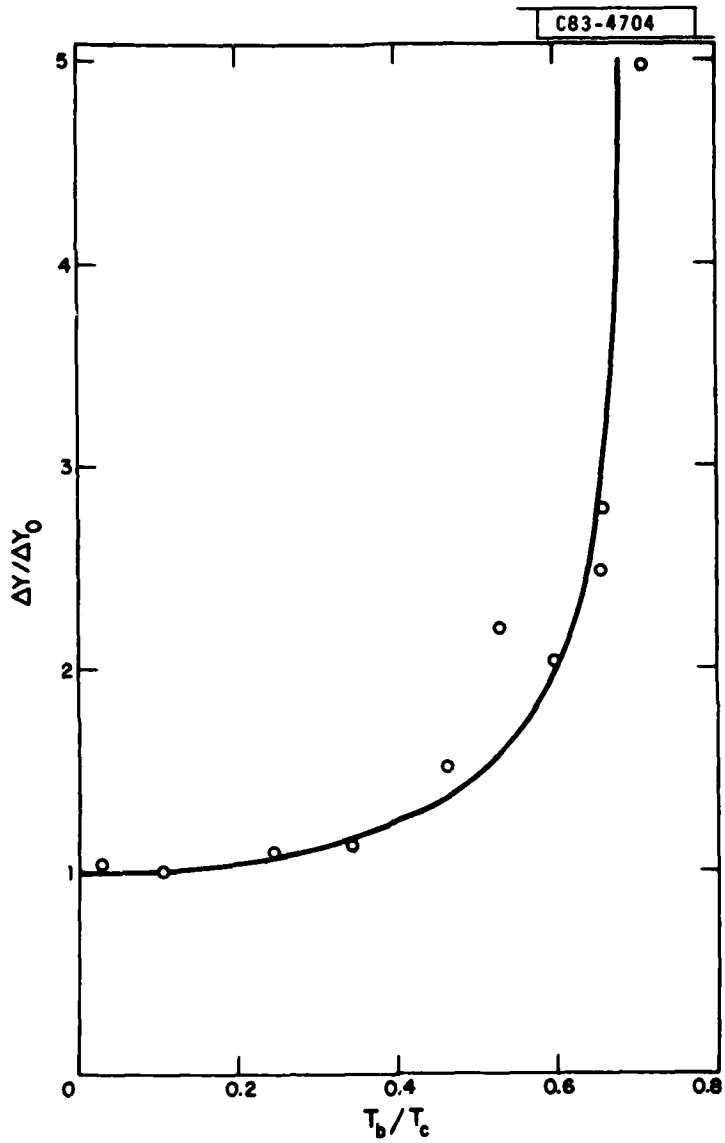

Fig. 6. Theoretical curve and experimental points for $\Delta Y/\Delta Y_0$ vs temperature ratio T_b/T_c. Curve is calculated using Fig. 5 with $\eta_0 = 0.22$ and $T_c = 685°C$.

transition temperature (937°C), and close to the value of ~ 680°C obtained from our analysis.

From the definition of η_0, $fL = \pi^{1/2} C T_c \eta_0$. Taking C = 0.08 cal/g°C for amorphous Ge (Ref. 3) and the values of T_c and η_0 used for Fig. 6, we obtain fL = 21.4 cal/g. In calorimetric measurements made during the rapid heating of amorphous Ge films, Fan and Anderson[4] observed a sharp transition at ~ 501°C and measured L = 39.8 cal/g. Using this value for L yields the result f ~ 0.54. The value of f obtained seems large, and is discussed further in Sec. IIIB.

The values of $S(\tau)$ plotted in Fig. 2 for the regions in which the phase boundary moves away from the laser image are not quantitatively correct, since the calculated values of S in this region increase more steeply as the size of the interval $\delta\tau$ chosen for the numerical integration of Eq. (3) is decreased. An examination of the integral equation indicates that in the beginning of these regions its solutions is singular and the initial velocity is infinite. This represents a limitation of the model since we have implicitly assumed that growth of the crystalline phase can follow at all times the requirements of the solution of the heat flow problem. In fact, the failure of this assumption may account for the presence of amorphous and fine-grained material in the initial portion of each periodic feature of the laser-crystallized films. Since the calculated values of S at which the boundary comes to rest approach a limit as $\delta\tau$ decreases, the computed spatial periods are reasonably reliable.

The Gaussian width of the laser temperature profile can be determined from the relationship $a = \Delta Y/V\Delta\tau$. From the measured $\Delta Y_0 = 50$ μm at room temperature and $V\Delta\tau \approx 0.3$ corresponding to $\eta_0 = 0.22$ in Fig. 5, a is ~ 170 μm, a reasonable value. The scanning velocity v corresponding to the normalized velocity V in our calculation can be obtained by using the relation $v = 4\kappa V/a$. A value for κ of ~ 0.09 cm^2/sec is estimated by taking $K = 0.035$ cal/cm sec°C,[13] $\rho \sim 5$ g/cm^3, and $C = 0.08$ cal/g°C. The value of normalized laser scan velocity used in our calculations, which was chosen for convenience in numerical integration, was $V = 0.3$. This corresponds to a laser scan velocity v of ~ 6 cm/sec, much higher than the actual value of 0.5 cm/sec used in our experiments. As indicated above, the results of our analysis of periodic a-c boundary motion are insensitive to the value of v assumed for the calculation as long as v is much less than the boundary velocity v_{ac}. For both runaway[6] and periodic motion[9] of the boundary, experimental values of v_{ac} lie in the range of 100 -300 cm/sec.

C. Temperature Distribution During Periodic Boundary Motion

Once the a-c boundary position as a function of time, $S(\tau)$, is known, Eq. (1) can be used to calculate the temperature at an arbitrary point S′ in the film at time τ. The resulting expression for the reduced temperature in terms of normalized quantities in the frame of reference moving with the laser is:

$$T'(S',\tau) = \alpha \exp\{-[S']^2\} + \eta \int_0^{\tau} \{[\dot{S}(\tau') + V]/(\tau-\tau')^{1/2}\} \times \left[\exp\{-\Gamma(\tau-\tau')\}\right]\left[\exp\{-[S' - S(\tau') + V(\tau-\tau')]^2/(\tau-\tau')\}\right] d\tau' \quad (5)$$

where the reduced temperature is

$$T'(S',\tau) \equiv \frac{T(S',\tau) - T_b}{T_c - T_b} .$$

It can be seen that when S' is the position of the a-c boundary, $S(\tau)$, $T(S',\tau) = T_c$, $T'(S',\tau) = 1$, and Eq. (5) becomes the integral equation (3). The numerical evaluation of Eq. (5) is discussed in Appendix A.

To illustrate the temperature fluctuations occurring during periodic boundary motion, we have used Eq. (5) to calculate $T'(S',\tau)$ as a function of S' for several fixed values of τ, for the case $\alpha = 3.6$, $\eta = 0.6$, $V = 0.3$, and $\Gamma = 30$. The results are shown in Fig. 7. It can be seen that during the forward motion of the a-c phase boundary, a temperaure pulse develops and propagates away from the center of the laser temperature profile. Before the pulse can escape, however, its motion stalls and it decays.

The case of the periodic fluctuations in light emission observed in some experiments is illustrated in Fig. 8 by the case $\alpha = 1.2$, $\eta = 0.6$, $V = 0.3$, and $\Gamma = 30$. In this case the laser temperature contribution is just barely large enough to initiate a-c boundary motion, and the latent heat released is enough to cause a sharp rise in temperature accompanied by the emission of

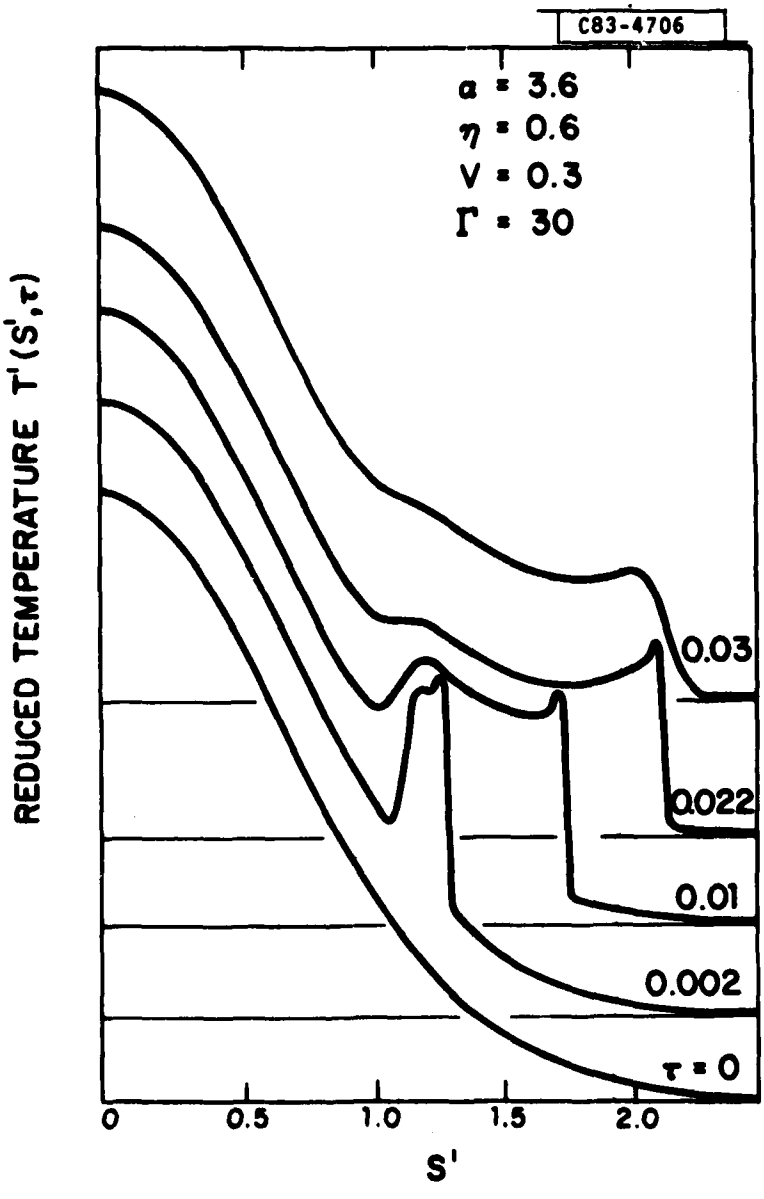

Fig. 7. Normalized temperature distribution $T'(S', \tau)$ as a function of S' for several values of τ. Parameters were chosen to illustrate the case of periodic a-c boundary motion.

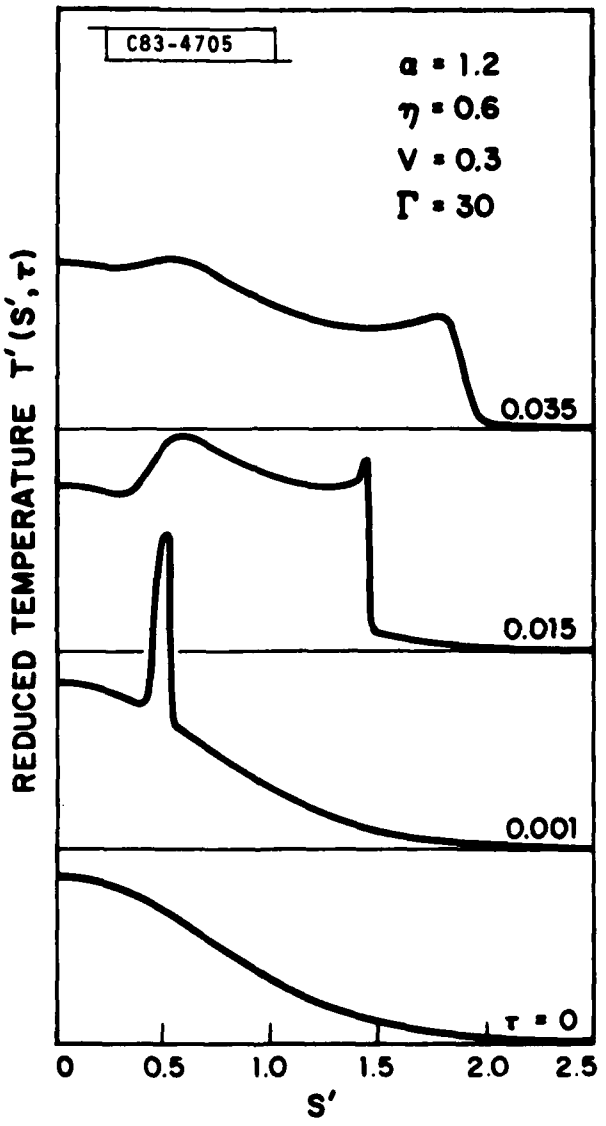

Fig. 8. Normalized temperature distribution $T'(S', \tau)$ as a function of S' for several values of τ, illustrating periodic temperature flare-up.

black body visible radiation. The peak temperature Tp reached can be calculated for this example by noting that

$$T_p = T_b + T_p' (T_c - T_b), \tag{6}$$

where T_p' is the peak value reached in Fig. 8. Equation (6) can be rewritten

$$T_p = T_c \left[\left(1 - \frac{\eta_0}{\eta}\right) + T_p'\left(\frac{\eta_0}{\eta}\right)\right] .$$

Using $T_c = 680°C$, $\eta_0 = 0.22$, $\eta = 0.6$, and $T_p' \approx 2.2$, we have

$$T_p \approx 986°C .$$

Although the numerical result is only approximate (since the computed velocity of the a-c boundary depends on the time interval $\delta\tau$ chosen for numerical integration), the calculation indicates that a large rise in temperature, and therefore light emission, can occur during a-c boundary motion.

III. Steady State Runaway Solutions

A. Integral Equation Model

As we have seen in Sec. IIA, for large enough values of η and relatively small values of normalized laser scan velocity V, the solutions of Eq. (3) are of the runaway type with the a-c boundary escaping from the region of the laser image and moving far ahead of it. In this case, Eq. (3) can be solved exactly without the need for numerical integration, by making the assumption that a steady state, constant velocity solution exists after

the passage of a long enough time τ_o. For the boundary far ahead of the laser image the laser contribution to Eq. (3) is negligible. We rewrite Eq. (3) at time τ_o in the frame of reference moving with the boundary at the normalized velocity $V_{ac} >> V$, with V_{ac} to be determined. In this frame of reference, V is replaced by V_{ac}, $S(\tau) = S(\tau')$, and $\dot{S}(\tau') = 0$ (since the solution is stationary). Equation (3) then becomes

$$1 = n \int_0^{\tau_o} [V_{ac}/(\tau - \tau')^{1/2}] \times \left[\exp\{-\Gamma(\tau-\tau')\}\right]\left[\exp\{-[V_{ac}(\tau-\tau')]^2/(\tau-\tau')\}\right] d\tau'. \quad (7)$$

Introducing the new variable $z^2 \equiv (\Gamma + V_{ac}^2)(\tau-\tau')$, Eq. (7) can be rewritten

$$1 = n \frac{V_{ac}}{[\Gamma + V_{ac}^2]^{1/2}} \times 2 \int_0^{[\Gamma + V_{ac}^2]^{1/2}\tau_o^{1/2}} e^{-z^2} dz$$

$$= n \pi^{1/2} \frac{V_{ac}}{[\Gamma + V_{ac}^2]^{1/2}} \operatorname{erf}\{[\Gamma + V_{ac}^2]^{1/2}\tau_o^{1/2}\}, \quad (8)$$

where $\operatorname{erf}\{x\} = \frac{2}{\sqrt{\pi}} \int_0^x e^{-z^2} dz$, the error function.

The error function approaches 1 for $x > 2$. Therefore, for

$[\Gamma + V_{ac}^2]^{1/2} \tau_o^{1/2} > 2$, Eq. (8) reduces to

$$1 = \eta\pi^{1/2} \frac{V_{ac}}{[\Gamma + V_{ac}^2]^{1/2}} \quad . \tag{9}$$

Equation (9) can be used to determine the runaway a-c boundary velocity V_{ac} from the values of η and Γ:

$$V_{ac} = \frac{\Gamma^{1/2}}{[\eta^2 \pi - 1]^{1/2}} \quad . \tag{10}$$

It can be seen that Eq. (10) has no solution for any value of V_{ac}, no matter how large, unless $\eta \pi^{1/2} > 1$, or $\eta > 0.56$.

In the runaway case, Eq. (5) for the reduced temperature distribution can also be evaluated exactly for large τ_o. In the same frame of reference moving with normalized velocity V_{ac}, Eq. (5) becomes

$$T'(S') = \eta \int_o^{\tau_o} [V_{ac}/(\tau-\tau')^{1/2}] \left[\exp \{-\Gamma (\tau-\tau')\}\right] \times \left[\exp \{-[S' + V_{ac} (\tau-\tau')]^2 / (\tau-\tau')\}\right] d\tau' \quad , \tag{11}$$

where S' is measured from the position of the a-c phase boundary. Eq. (11) can be written,

$$T'(S') = \eta \frac{V_{ac}}{[\Gamma + V_{ac}^2]^{1/2}} \times 2\, e^{-2S' V_{ac}} \int_0^{[\Gamma + V_{ac}^2]^{1/2} \tau_0^{1/2}} e^{-z^2}\, e^{-q^2/z^2}\, dz, \quad (12)$$

where $q^2 = S'^2 [\Gamma + V_{ac}^2]$.

Using the known definite integral,

$$\int_0^\infty e^{-p^2 z^2}\, e^{-q^2/z^2}\, dz = \frac{\sqrt{\pi}}{2p}\, e^{-2pq}, \quad (p,q > 0)$$

we obtain, for large τ_0,

$$T'(S') = \eta \pi^{1/2} \frac{1/2\, V_{ac}}{[\Gamma + V_{ac}^2]^{1/2}}\, e^{-2S' V_{ac}}\, e^{-2[\Gamma + V_{ac}^2]^{1/2} |S'|} . \quad (13)$$

For $S' = 0$, corresponding to the position of the a-c boundary, $T'(S') = 1$, and Eq. (13) reduces to Eq. (9), as it should.

To explore the approach to the steady-state runaway temperature distribution, we have used the values of $S(\tau)$ obtained from numerical integration of Eq. (3) for $\alpha = 2.0$, $\eta = 0.8$, $V = 0.3$, and $\Gamma = 30$, to calculate

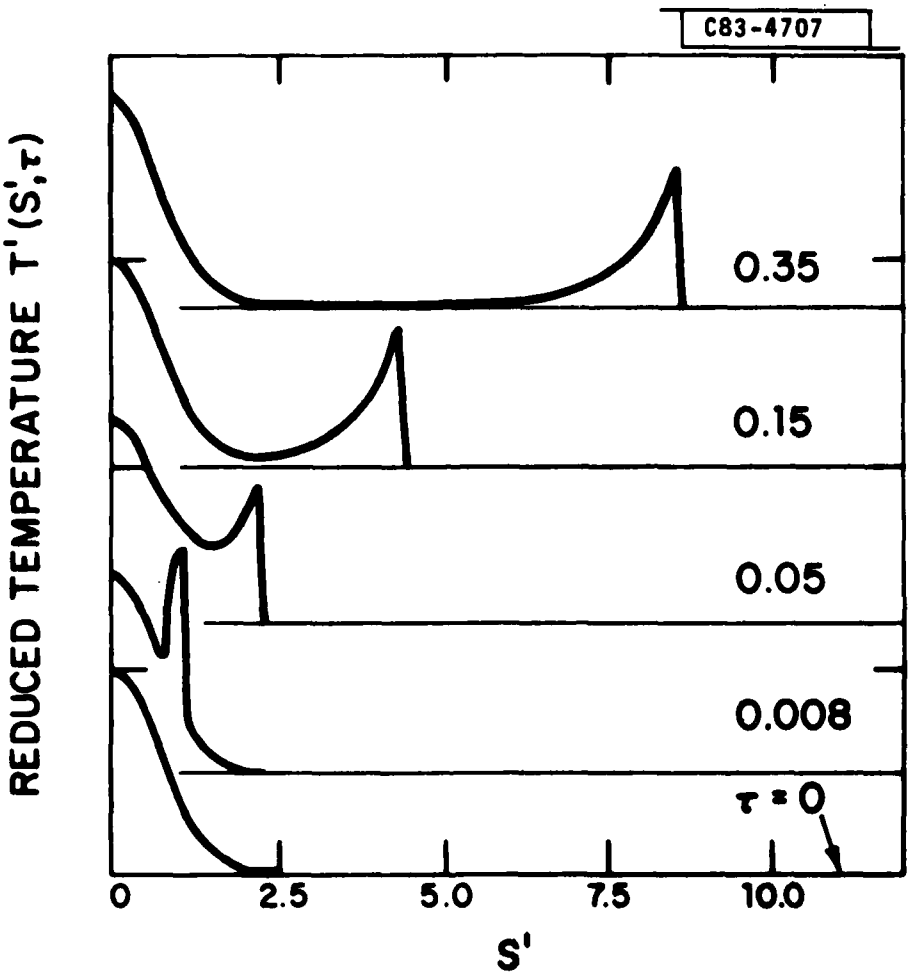

Fig. 9. Normalized temperature distribution $T'(S', \tau)$ as a function of S' for several values of τ. The parameter values $\alpha = 2.0$, $\eta = 0.8$, $V = 0.3$ and $\Gamma = 30$ have been chosen to illustrate the case of runaway.

$T'(S',\tau)$ from Eq. (5) for several values of τ. The results are shown in Fig. 9. In contrast to the periodic solution case shown in Fig. 7, the a-c boundary in the runaway case develops a well-defined peak-structure in $T'(S',\tau)$, which propagates away from the laser image as τ increases. The velocity of propagation of the a-c boundary and the amplitude and shape of the propagating temperature pulse shown in Fig. 9 are not in agreement with the exact limiting results given by Eqs. (10) and (13), respectively. Thus, from Eq. (10) with $\Gamma = 30$ and $\eta = 0.8$ we have the exact normalized velocity $V_{ac} = 5.45$, much less than the normalized velocity obtained from numerical integration and indicated by Fig. 9. These discrepancies may in part be due to computational problems, but may also be due to a slow approach to the steady state. (It should be noted that at the maximum $S(\tau)$ shown, the a-c boundary has moved only a few times the Gaussian width, ~ 170 μm, from the laser beam.)

B. Two-Dimensional Solution

In Appendix B we obtain expressions for the temperature distribution in the steady state a-c boundary runaway condition for a semiconductor film as a function of normalized distance S' from the boundary by the solution of a two-dimensional bounary value problem. In this treatment the flow of heat into the substrate is handled exactly, and it is not necessary to introduce ad-hoc parameters equivalent to f and γ of the one-dimensional integral equation model. The solution of the problem is discussed in Appendix B.

Equations (B31a) and (B31b) give the temperature distribution $T_1(S')$ in the semiconductor film of thickness b_1 supported on a substrate of thickness b_2 as a function of steady state velocity V of the a-c boundary. If the a-c boundary is at a temperature T_c, then we can rewrite Eqs. (B31a) and (B31b) in the form

$$T'(S') = \pi' V_{ac}\, \pi^{1/2} \sum_{n_+} \frac{e^{-2V_{ac}S'} e^{-2[\Gamma_{n+} + V_{ac}^2]^{1/2}\,|S'|}}{[\Gamma_{n+} + V_{ac}^2]^{1/2}} f_{n^+}(V_{ac}) \,, (S' < 0) \tag{14a}$$

$$T'(S') = \pi' V_{ac}\, \pi^{1/2} \sum_{n_-} \frac{e^{-2V_{ac}S'} e^{-2[\Gamma_{n-} + V_{ac}^2]^{1/2}\,|S'|}}{[\Gamma_{n-} + V_{ac}^2]^{1/2}} f_{n^-}(V_{ac}), \; (S' > 0) \tag{14b}$$

where

$$T'(S') = \frac{T_1(S') - T_b}{T_c - T_b} \,,$$

$$\pi' = \frac{L}{\pi^{1/2} C_1 (T_c - T_b)} \,, \tag{14c}$$

$$f_{n\pm}(V) = \frac{1}{\left[1 - \beta/2 \left\{\frac{\cot Q_{n\pm}}{Q_{n\pm}} - \csc^2 Q_{n\pm}\right\} \left\{1 \pm \frac{V(M-1)}{\sqrt{(\Gamma_{n\pm} + V^2)}}\right\}\right]} \,,$$

$\beta = K_2 b_2 / K_1 b_1$ and $M = \kappa_1 / \kappa_2$, and S' is the normalized distance from the a-c boundary, V_{ac} is the normalized a-c boundary velocity. For the normalization unit of length d we use b_2. Subscripts 1 and 2 refer to laser

crystallized film and substrate, respectively. The Γ_{n+} and Γ_{n-} are roots of a transcendental equation, (B26b), and the $Q_n\pm$ are given by the expression (B26a) evaluated for $\Gamma_n\pm$.

One case for which the solution of Eqs. (14a) and (14b) can be readily evaluated is a thin amorphous film on a thick substrate with identical thermal properties ($M = 1$, $\beta = b_2/b_1 >> 1$). For this case,

$$f_{n+} = f_{n^-} = 2/\beta; \quad \Gamma_{n^+} = \Gamma_{n^-} = (2n + 1)^2\pi^2/16.$$

The general condition determining the steady state a-c boundary velocity V_{ac} is that at $S' = 0$, $T'(0) = 1$ or,

$$1 = n'V_{ac}\pi^{1/2} \sum_{n+} \frac{f_{n+}(V_{ac})}{[\Gamma_{n^+} + V_{ac}^2]^{1/2}} = n'V_{ac}\pi^{1/2} \sum_{n-} \frac{f_{n-}(V_{ac})}{[\Gamma_{n^-} + V_{ac}^2]^{1/2}} . \qquad (15)$$

It is interesting to compare the results of Eqs. (14) and (15) with the one-dimensional integral equation results of Eqs. (13) and (9), respectively. Noting that $n = fn'$, it can be seen that Eqs. (13) and (9) represent approximations in which single average terms have replaced sums of terms of the same form in the two dimensional result.

We define the functions in the summation in Eq. (14a) and (14b) as

$$F^{\pm}(S',V) \equiv \sum_{n\pm} \frac{e^{-2VS'} e^{-2[\Gamma_{n\pm} + V^2]^{1/2} |S'|}}{[\Gamma_{n\pm} + V^2]^{1/2}} f_{n\pm}(V). \qquad (16)$$

$F^{\pm}(S',V)$ is proportional to the steady-state temperature distribution due to a slit image source of heat scanned with normalized velocity V along the surface of a semiconductor film. When evaluated for $V = V_{ac}$, it yields the shape of the distribution for a-c boundary runaway. We have evaluated Eq. (16) as a function of S' for a number of values of V for the case of a thin film of Ge on a fused silica substrate, since the experimental results reported in Sec. II B were obtained for this case. The values of $K_1 = 0.035$ cal/cm sec^{o}C, $\kappa_1 = 0.09$ cm^2/sec and $K_2 = 0.0025$ cal/cm sec^{o}C, $\kappa_2 = 0.005$ cm^2/sec were those for Ge (1), and fused silica (2). The thicknesses used in the calculation, appropriate to our experiments[7] were $b_1 = 0.3$ μm for Ge and $b_2 = 1$mm for fused silica. With these values, $\beta \cong 240$, and $M \cong 18$.

Figure 10 shows $F(S',V)$ as a function of S' for several values of V. For $V \gtrsim 0.1$, the leading edge of the temperature distribution begins to sharpen, and the peak value begins to drop. This is an indication that V has reached a value at which diffusion of heat can no longer restore the static temperature distribution as the heat source moves. It should also be noted that the fact the two portions of the curves of $F^{\pm}(S',V)$ meet at $S' = 0$ is a significant check on the correctness of the numerical calculation, since the

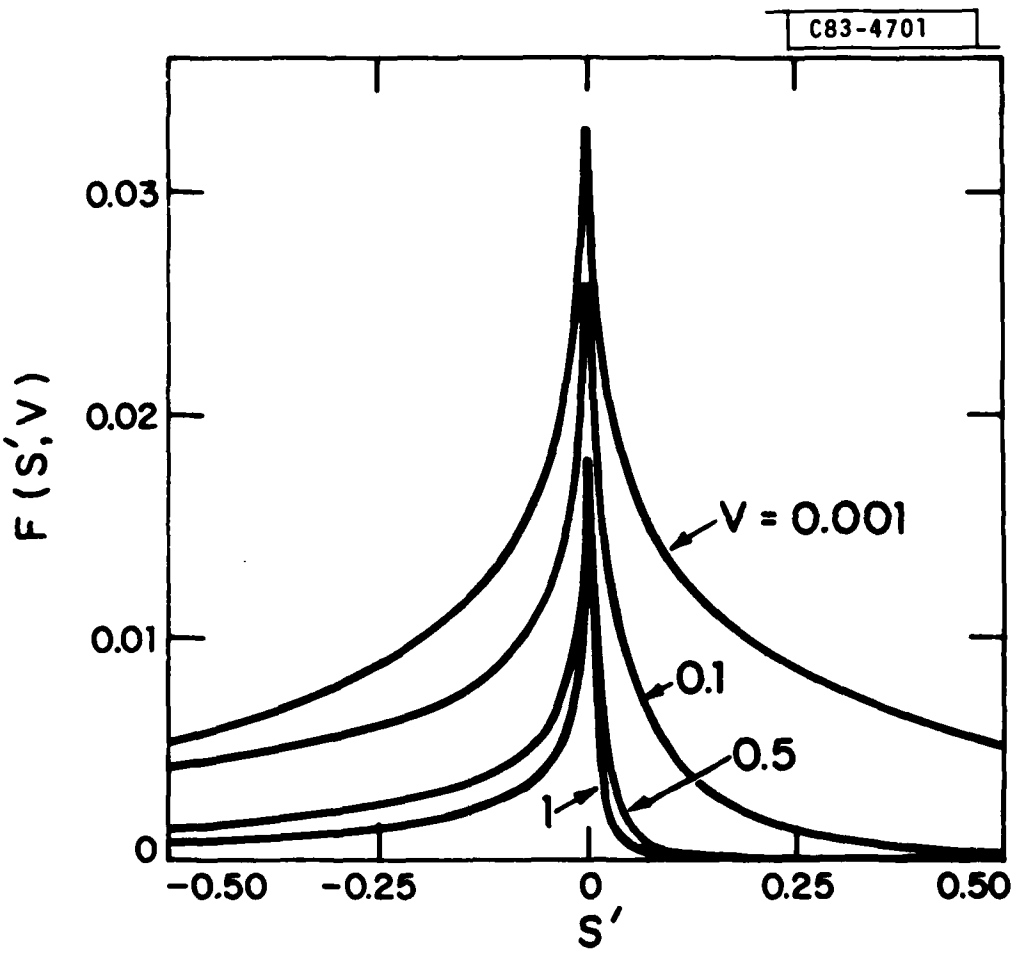

Fig. 10. F(S′, v) as a function of S′ for several values of V.

formal expressions for $[F^+(S',V)]_{S'} = 0$ and $[F^-(S',V)]_{S'} = 0$ are not identical.

To obtain quantitative results for V_{ac}, we make use of Eq. (15) and assume that Tc is a fixed transition temperature (modification of this assumption is discussed in Sec. V). The relation to be solved for V can be written,

$$\pi^{1/2}\eta' V_{ac} = [F(0, V_{ac})]^{-1} \quad . \tag{17}$$

We plot log $[F(0,V)]^{-1}$ vs log V and log $[\pi^{1/2}\eta' V]$ vs log V on the same graph. The solution for V_{ac} will be given by the intersection of the two curves. Figure 11 shows $[F(0,V)]^{-1}$ for M = 18, and for several values of β. We consider first the curve for $\beta = 240$, corresponding to our experiment. One of the straight lines shown gives log $[\pi^{1/2}\eta' V]$ for $\eta' = 2.2$, and we see that there is no solution for this value of η'. The minimum value of η' for a steady state solution, η'_{min}, corresponds to the lowest temperature (T_r) at which runaway can occur. This solution is obtained when the two curves first cross, and is found to occur when $\eta' \cong 6.1$. For values of η' greater than 6.1, there are steady state or runaway solutions for V_{ac} which decrease with increasing η'. It should be noted that the two curves first make contact tangentially as η' increases to η'_{min}. This is similar to the integral equation result, Eq. (10).

It is difficult to identify the first true "crossing" point for two curves that approach each other tangentially. Roughly, for $\eta' \cong 6.1$ the two

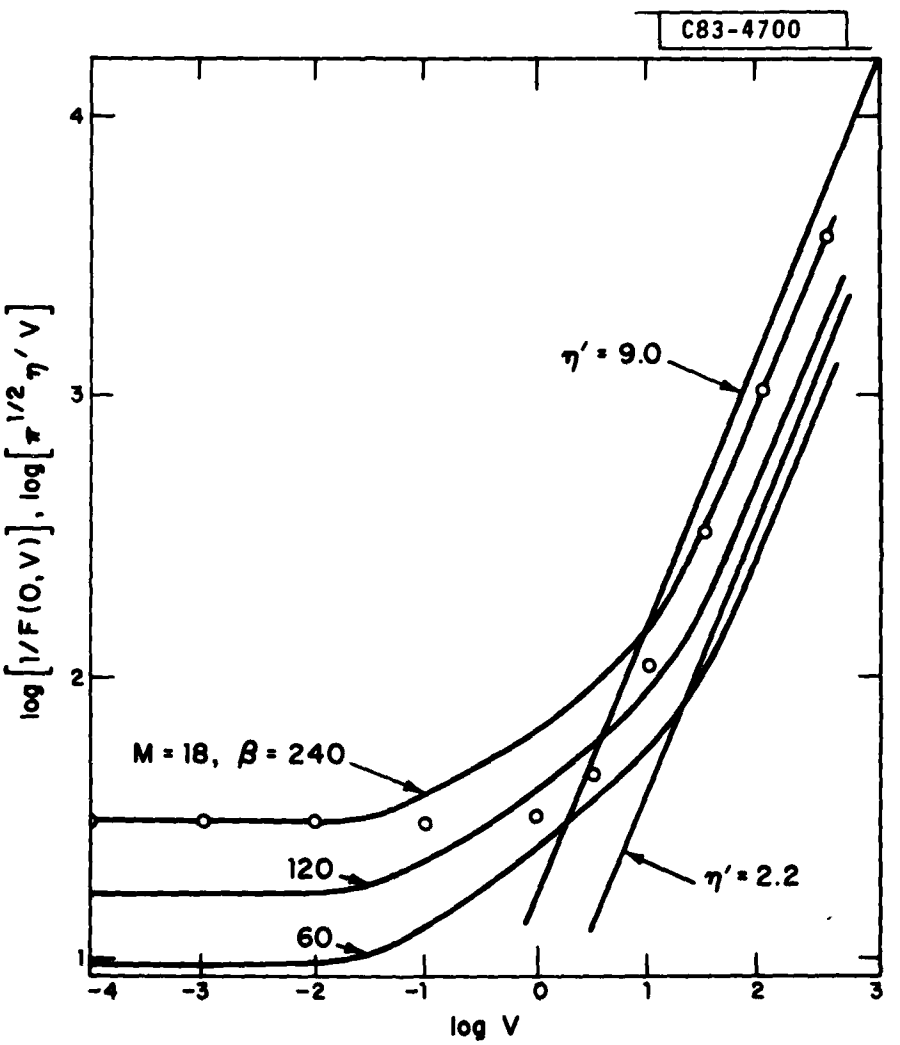

Fig. 11. Plots of log [F(0, V)] vs log V for β = 240, 120, and 60, and plots of log [$\pi^{1/2}$ η'V] vs log V for η' = 9.0 and η' = 2.2.

curves cease to run parallel for log V ~ 1.6. Using the relation $v \sim 4\kappa_1 V/b_2$, with $\kappa_1 = 0.09$ cm^2/sec, and $b_2 = 10^{-1}$ cm, we find, $v_{ac} \cong 140$ cm/sec. Larger values of η' should lead to smaller values of v_{ac}, consistent with the integral equation result, Eq. (10).

From the relation (14c), we can calculate the value of T_c if we equate η' with $\eta'_{min} = 6.1$ and T_b with the experimental value of T_r, ~ 500°C. This leads to $T_c \sim 550$°C, much lower than the value of ~ 680°C obtained from the fit of the periodicity data to the theoretical results obtained from the integral equation model. As we shall see shortly, the discrepancy can be explained qualitatively by the presence of a thermal barrier between film and substrate.

We can attempt to approximate the calculated F(0,V) in the form

$$F(0, V) \cong f/[\Gamma + V^2]^{1/2} \quad , \tag{17a}$$

where f and Γ are to be determined for the best fit. Equation (17) would then be precisely of the form Eq. (9), obtained from the integral equation, where $\eta = f\eta'$. The open circles in Fig. 11, representing Eq. (17a) with $\Gamma = 7.95$ and $f = 0.093$, fit the calculated curve of log $[F(0,V)]^{-1}$ with $\beta = 240$ and $M = 18$ for small V and large V, but fit poorly in between. This value of f is much lower than that obtained from the integral equation fit to the periodicity data, $f \sim 0.58$. As we shall see shortly, this descrepancy can also be qualitatively explained by the presence of a thermal barrier between film and substrate.

We have examined the effect of changing b_1 and b_2 on the values of a number of properties of a-c boundary runaway. Figure 11 shows plots of log $[F(0,V)]^{-1}$ vs log V for M = 18 and β = 120 and 60, in addition to the curve for β = 240, which corresponds to our experiment. We can interpret the reduction in β as due to either a decrease in b_2 or an increase in b_1. The results obtained for V_{ac} and v_{ac} for $\eta' = 9.0$ (corresponding to fixed T_b, and well above η'_{min} for all 3 values of β) are listed in Table I. It can be seen that for b_1 held fixed at 0.3 μm , v_{ac} decreases only slightly as b_2 decreases. On the other hand, for b_2 held fixed at 10^3 μm, v_{ac} decreases almost inversely with increasing b_1. However, in most cases it might be difficult to see this striking drop in v_{ac}, since at temperatures above T_r, spontaneous fluctuations can cause the a-c transformation (see Sec. V.)

Also shown in Table I are values of η'_{min}, with corresponding values for V_{ac} and v_{ac}, as well as approximate values of f and Γ. It can be seen that f increases nearly inversely as β decreases, while Γ increases slowly. It should also be noted that η'_{min} decreases as b_1 increases. This means that the lowest value of T_b for runaway, T_r, decreases as film thickness increases. As the film thickness b_1 increases, the velocity v_{ac} for η'_{min} increases, but remains in the range of 100-300 cm/sec.

The small values obtained for T_c and f by applying the present theory directly to experiment can be understood if we postulate the presence of a thermal barrier between the fused silica substrate and the amorphous Ge film in our laser crystallization experiments.[7] The presence of a thermal barrier

TABLE I

Results of Two Dimensional Solution for a-c Boundary Motion

Values of a number of quantities calculated from exact solutions of a model of laser crystallization, as obtained from Fig. 11. For three values of the parameter β, effective parameters f and Γ and the minimum value of η' for runaway, η'_{min}, are given. With $\eta' = \eta'_{min}$ and $\eta' = 9.0$, normalized velocities V_{ac} for a-c boundary runaway are obtained. For combinations of substrate (b_2) and film (b_1) thicknesses given, these values of V_{ac} lead to the a-c boundary runaway velocities v_{ac} that are shown.

β	f	Γ	η'_{min}	V_{ac} ($\eta'=\eta'_{min}$)	V_{ac} ($\eta'=9.0$)	b_2 (μm)	b_1 (μm)	v_{ac}(cm/sec) ($\eta'=\eta'_{min}$)	v_{ac}(cm/sec) ($\eta'=9.0$)
240	0.093	7.95	6.1	39	10	10^3	0.3	140	36
120	0.178	8.72	3.2	47	4.07	10^3	0.6	170	14.7
						5×10^2	0.3		29.3
60	0.331	10.15	1.7	71	1.9	10^3	1.2	255	6.8
						2.5×10^2	0.3		27.4

is not at all unreasonable, and could be readily included in the derivation of modified equations (14a) and (14b). The effect of a thermal barrier is approximately equivalent to decreasing the thermal conductivity of the substrate, and is therefore qualitatively described by decreasing β (although the thermal conductivity ratio appears in M, this describes the way heat diffuses once it is transferred to the substrate and should therefore be kept fixed for this crude argument). To obtain a rough idea of the effect of such a barrier, we examine the effect of decreasing β by comparing the results for $\beta = 240$ with those obtained for $\beta = 60$. Referring to table I, we see that for $\beta = 60$, f has increased to 0.331, much closer to the empirical value 0.58 determined from the experimental data by comparison with the one-dimensional integral solution. Furthermore, η'_{min} has dropped from 6.1 to 1.7, yielding a value of $T_c \cong 665°$ determined from equation (14c). This is close to the value of 680° C obtained from the fit of experimental data to the integral equation model. While this argument is very crude, it does suggest that the presence of a thermal barrier can eliminate the discrepancy between experimentally determined parameters and the results of a first-principles calculation.

IV. Steady State Laser-Guided Solutions

An intriguing class of steady state solutions exists in which the a-c boundary proceeds at a constant velocity on the leading edge of the scanning laser image. Solutions of this type will be obtained for both the integral

equation model and the two-dimensional model of the a-c boundary motion. The laser-guided mode of a-c transformation could have important implications for the controlled growth of semiconductor films. The question of the initial conditions which permit the system to settle into the steady state laser-guided mode of motion will be discussed in Sec. V.

A. Integral Equation Model

To find laser-guided solutions, we rewrite Eq. (3) in the frame of reference, moving at normalized velocity V, in which the laser and a-c boundary temperature distributions are stationary. The result is

$$1 = T_{\ell}'(0) + \eta \int_0^{\tau_0} [V/(\tau-\tau')^{1/2}] \left[\exp\{-\Gamma(\tau-\tau')\}\right] \times \left[\exp\{-[V(\tau-\tau')]^2/(\tau-\tau')\}\right] d\tau' \quad , \tag{18}$$

where $T_{\ell}'(0)$ is the reduced temperature due to the scanning laser image at the positon of the a-c boundary, $T_{\ell}'(0) = T_{\ell}(0)/(T_c-T_b)$.

As in Sec. III A, the integral in Eq. (18) can be evaluated exactly for large enough τ_0, and we find

$$1 = T_{\ell}'(0) + \eta V \pi^{1/2} / [\Gamma + V^2]^{1/2} \quad . \tag{19}$$

According to Eq. (19), for values of η and V such that $\eta V \pi^{1/2}/[\Gamma + V^2]^{1/2} < 1$, there is a value of $T_{\ell}'(0)$ which will satisfy the condition for a laser-guided solution. For given values of V (determined by laser scan

velocity) and η and a given reduced temperature profile due to the laser, the (a-c) boundary will ride at a distance in front of the laser image such that Eq. (19) is satisfied. It should be noted that solutions of Eq. (19) exist for values of V arbitrarily small. The question of coupling into such solutions in real situations is discussed in Sec. V.

B. Two-Dimensional Solution

It is a straightforward matter to show that the two-dimensional solution of the laser crystallization problem also leads to laser-guided stationary solutions. As shown in Appendix B, the solution of the steady state temperature distribution for the boundary value problem in the presence of several heat sources is the superposition of the solutions in the presence of the individual heat sources. In the presence of both a laser source of heat and the heat source due to the moving a-c boundary, the solution for steady state runaway, Eq. (15), becomes

$$1 = T_{\ell}'(0) + \eta\sqrt{V\pi}^{1/2} \sum_{n+} \frac{f_{n+}(V)}{[\Gamma_{n+} + V^2]^{1/2}}$$

$$= T_{\ell}'(0) + \eta\sqrt{V\pi}^{1/2} \sum_{n-} \frac{f_{n-}(V)}{[\Gamma_{n-} + V^2]^{1/2}} \quad , \tag{20}$$

where $T_{\ell}'(0)$ is the reduced temperature due to the scanning laser image at the position of the a-c boundary. The close correspondence between the two-dimensional solution Eq. (20) and the integral equation solution Eq. (19) should be noted.

Using the definition of $F^{\pm}(S',V)$, Eq. (16), we obtain for the laser-guided problem an expression analogous to Eq. (17), which was solved to determine V_{ac} for runaway. The result is

$$\frac{\pi 1/2 \eta' V}{1-T_{\ell}'(0)} = [F(0,V)]^{-1} \quad . \tag{21}$$

We may think of $\eta'/[1-T_{\ell}'(0)]$ as an effective value, η'_{eff}. Referring to Sec. III B and Fig. 11, it can then be seen that by decreasing $1-T_{\ell}'(0)$, the normalized laser scan velocity V for laser-guided steady state solutions can be reduced greatly. For a given reduced temperature distribution due to the laser scanning at velocity V, the a-c boundary rides at a point in front of the laser image satisfying Eq. (21).

V. Discussion

One of the important assumptions made in calculating the motion of the a-c boundary for both the one-dimensional integral equation and two-dimensional solution was the existence of a sharply defined transition temperature T_c. In fact, the velocity of growth of crystalline material directly from the amorphous state, $\dot{S}(T)$, is a function of temperature, increasing rapidly as the temperature is raised. This could be interpreted as determining the temperature $T_c(\dot{S})$ at which the transition can take place at a value of $\dot{S}$ demanded by the heat flow calculation. From this simplistic point of view, over a wide range of values of $\dot{S}$, T_c varies relatively little and can be taken as constant. As already pointed out in Sec. II B, the model solution

of the integral equation at the beginning of each period of boundary motion requires infinite velocity, and the presence of amorphous and fine-grained material in the initial portion of each period may be related to the limits on the rate at which crystalline growth can occur.

We could attempt to improve the approximate description of the boundary motion using the integral Eq. (3) by replacing n by the quantity

$$n_{eff}(\dot{S}) = f\, L(\dot{S})/[T_c(\dot{S}) - T_b]\,, \tag{22}$$

where $T_c(\dot{S})$ is the critical temperature appropriate to the value of $\dot{S}$, and $L(\dot{S})$ is an effective latent heat which is that portion emitted when partial conversion to crystalline material takes place at boundary velocity $\dot{S}$. We now interpret $\dot{S}$ as the velocity of a "heat flow boundary", which is identical to the a-c boundary when that boundary is well defined. We can see that at large $\dot{S}$, $n_{eff}(\dot{S})$ is reduced because $L(\dot{S})$ is reduced and $T_c(\dot{S})$ is increased. At lower values of $\dot{S}$, $L(\dot{S}) \to L$, and $T_c(\dot{S}) \sim T_c$. The introduction of an $n_{eff}(\dot{S})$ of this form could eliminate the unphysical singularity in the initial motion present in Eq. (3), while still yielding a very high initial value of $\dot{S}$, consistent with the initial amorphous and fine-grained polycrystalline material in each period. The introduction of an $n'_{eff}(V_{ac})$ in Eq. (17) would also modify the exact solutions obtained for V_{ac} from the boundary value problem.

As mentioned in Sec. II B, the value of T_c obtained by fitting the results of the integral equation solution to our experimental data was

T_c ≈ 680°C, very close to the value of 696°C predicted by Bagley and Chen[10] for the transition temperature from the amorphous to liquid state of Ge. It has been suggested[14,15] that "explosive" crystallization (or runaway) may correspond to the occurrence of this transition, and some experimental evidence supporting this point of view has been obtained.[16] If, in fact, T_c does correspond to the amorphous-to-liquid transition, the assumption of a fixed T_c over a range of $\dot{S}$ is reasonable. Once the transition from the amorphous to the liquid state had occurred, the unstable liquid would rapidly transform to the crystalline state.[10] For small temperature differences across a thin liquid layer, the treatment we have presented would then require no major modification.

Throughout this paper, we have treated the amorphous and crystalline regions of the semiconductor film undergoing laser crystallization as istropic and homogeneous regions, with the transformation from the amorphous to the crystalline state governed by macroscopic heat flow equations. An important ingredient absent from this description, and essential for even a qualitative understanding of crystallized film morphology, is the role of nucleation centers[17] and "nucleation events". Because the exact nature of the a-c transformation in laser crystallization is not yet certain, we will not attempt a detailed description of nucleation. We regard a nucleation event as a spontaneous, localized fluctuation which initiates a transformation from the amorphous to the crystalline state and produces a small increase in local temperature above the background determined by macroscopic heat flow. A

nucleation event has a probability of occurrence which increases with the density of nucleation centers (which depends on film perfection) and with increasing temperature. For T_b just below T_r, the lowest temperature for runaway, nucleation events can produce transformation from the amorphous to crystalline state in small regions of finite range about nucleation centers.[18] For $T_b \sim T_r$ and in the absence of an external disturbance such as a laser beam, multiple nucleation events can occur, overlapping and spontaneously transforming the entire film to the crystalline state in a short time if the probability of such events is high enough. From the discussion of Sec. III B, the lowest value of T_b for runaway, T_r, is higher for thinner films, decreasing as the films become thicker. Since the probability of nucleation events increases with increasing temperature, spontaneous transformation to the crystalline state should occur most readily at $T_b \sim T_r$ for thin amorphous films. This is consistent with our observation of laser-induced runaway for films of thickness greater than 1 μm, while only spontaneous transformation is observed for films 0.3 μm thick.

The occurrence of nucleation events appears to play a major role in the morphology of laser-crystallized films. In the films that we have examined in detail, the elongated crystallites within each periodic feature form a roughly chevron-like pattern, with the two halves of the pattern symmetrical about an axis that is parallel to the laser scan direction and located near the center of the laser image. The elongated crystallites on each side of the pattern have their long axes aligned along [100] directions. A blown-up picture of a

crystallized film near the center axis of the chevron pattern is shown in Fig. 12. The "origin" of the chevron pattern within each periodic feature is a small region located somewhere near the center axis. The exact lateral position of the origin varies from one period to the next over a distance of perhaps 100 μm (~ 10% of the slit image length). This suggests that the origin represents the position of the first nucleation event within a periodic feature where the heat flow boundary is moving slowly enough for large crystallites to form. The first nucleation event would be likely to occur near the center axis, since the laser slit image is an ellipse of high aspect ratio and the temperature should therefore first reach T_c near this axis. Once nucleation and growth of large crystallites began, heat would flow forward, but also laterally, raising the temperature and inciting the nucleation of new growth centers laterally. The direction of growth from these centers would tend to be channeled by such factors as interaction with neighboring crystallites already formed,[19] strong anisotropy in the directional dependence of growth rate, and perhaps stresses in the film. The result of all of these influences would combine in a statistical way, but it can be argued that the outcome would be largely determined by the tendency of growth to occur along the direction of the temperature gradient at the a-c boundary, combined with the high rate of growth along a [100] direction compared to other crystallographic directions. Motion of the a-c boundary would occur laterally as well as along the laser scan direction, but a periodic morphological pattern would still result. This description is

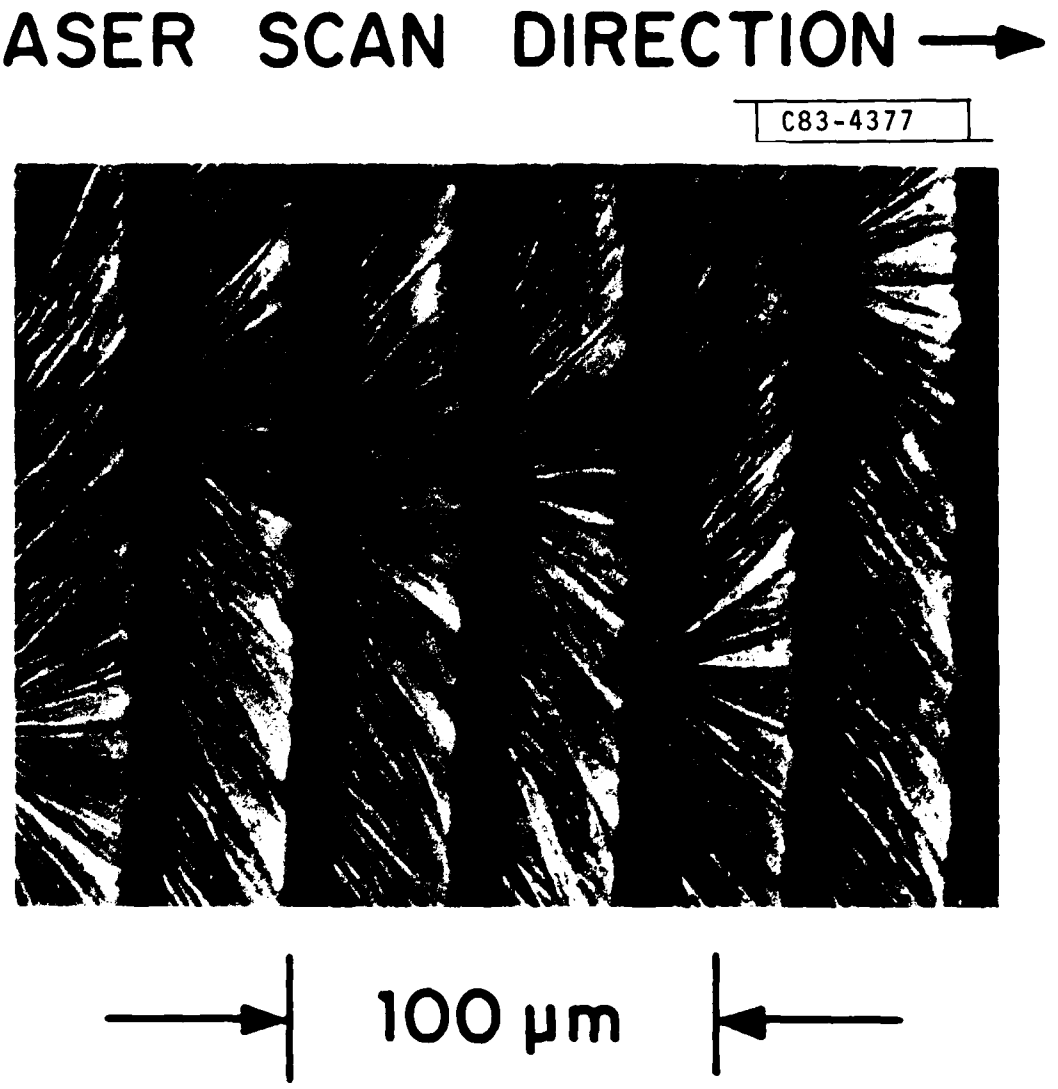

Fig. 12. Blown up view of periodic features in a Ge film crystallized by the slit image of a laser. Picture taken near the center axis of the slit image shows the origins of chevron pattern.

consistent with the observed chevron pattern, and could serve as the basis for a more complete analysis.

In Sec. IV we discussed a class of laser guided stationary solutions of both the integral equation formulation and the two-dimensional formulation of a-c boundary motion. The problem remains of identifying spatial and temporal initial conditions which allow the boundary motion to settle into such a constant velocity stationary state. The solution of this problem could have important implications for the possibility of producing uniformly aligned, laser crystallized semiconductor films. In studying solutions of the integral Eq. (3), as discussed in Sec. IIA, we noted that for a given interval $\delta\tau$ used in numerical integration, values of normalized laser scan velocity V could be found which were large enough to generate damped oscillatory behavior in $S(\tau)$. After a few cycles, $S(\tau)$ settled down to a constant value, consistent with the a-c boundary riding at a fixed distance in front of the scanning laser image, as expected in a laser-guided stationary solution. However, if V was now held fixed and $\delta\tau$ decreased further, the damped oscillatory behavior was again replaced by perodic relaxation oscillation behavior of the type shown in Fig. 2 for $\eta = 0.3$ or 0.6. These numerical results are to be expected, since a given value of $\delta\tau$ gives rise to an effective finite initial velocity V_{eff} of the a-c boundary, and for a value of laser velocity $V > V_{eff}$, damped oscillatory motion should result. On the other hand, Eq. (3) is characterized by singular behavior of the initial velocity, so that decreasing $\delta\tau$ sufficiently will increase V_{eff} to the point where $V_{eff} > V$, and the a-c

boundary again outruns the laser, resulting in periodic relaxation oscillations. As we have seen, this singular behavior of the initial velocity of the a-c boundary is unphysical, and would probably be eliminated from the mathematical description by replacing n in Eq. (3) by a velocity dependent n_{eff} given by Eq. (22). Under these circumstances, the nature of the solution obtained should not depend on the interval $\delta\tau$ chosen for numerical integration, provided that $\delta\tau$ was sufficiently small. The argument implies that for a small value of laser scan velocity V, the initial motion of the a-c boundary would be characterized by some finite velocity V_0. For laser scan velocity $V > V_0$, we would then expect a damped oscillatory behavior of $S(\tau)$, with the motion settling into a laser-guided stationary state. A slow decrease in V could perhaps then lead the a-c boundary motion into a laser-guided stationary state at a lower velocity, with the a-c boundary riding close to the thermal image of the scanning laser. However, the stability of such states remains questionable. All of these points are highly speculative, and require further exploration.

Acknowledgements

We are grateful to A. J. Strauss for his interest, advice, and encouragement during the entire course of this research. We wish to thank Ms. Elaine Aalerud and Ms. Linda Oakley for their patience and skill in the preparation of this report. This research was supported by the Department of the Air Force, the Solar Energy Research Institute, and the Department of Energy.

References

1. N. A. Blum and C. Feldman, J. Non-Cryst. Solids 22, 29 (1976).
2. N. A. Blum and C. Feldman, J. Non-Cryst. Solids 11, 242 (1972).
3. H. S. Chen and D. Turnbull, J. Appl. Phys. 40, 4214 (1969).
4. J. C. C. Fan and C. H. Anderson, J. Appl. Phys., to be published, June 1981.
5. See for example, T. Takamori, R. Messier, and R. Roy, Appl. Phys. Lett. 20, 201 (1972); K. J. Callanan, A. Matsuda, A. Mineo, T. Kurosu, and M. Kikuchi, Solid State Commun. 15, 119 (1974); C. E. Wickersham, G. Bajor, and J. E. Greene, Solid State Commun. 27, 17 (1978).
6. A. Mineo, A. Matsuda, T. Kurosu, and M. Kikuchi, Solid State Commun. 13, 329 (1973).
7. J. C. C. Fan, H. J. Zeiger, R. P. Gale, and R. L. Chapman, Appl. Phys. Lett. 36, 158 (1980).
8. H. J. Zeiger, J. C. C. Fan, B. J. Palm, R. P. Gale, and R. L. Chapman in Proceedings of Symposium on Laser and Electron Beam Processing of Materials, C. W. White and P. S. Peercy, Eds. (Academic Press, New York, 1980), p. 234.
9. R. L. Chapman, J. C. C. Fan, H. J. Zeiger, and R. P. Gale, Appl. Phys. Lett. 37, 292 (1980).
10. B. G. Bagley and H. S. Chen, A.I.P. Conference Proceedings No. 50, Laser-Solid Interactions, Ferris, Leamy, and Poate, Eds. (Boston, 1978), p. 97.

11. H. S. Carslaw and J. C. Jaeger, Conduction of Heat in Solids (Oxford University Press, London, 1959), p. 293.

12. M. W. Geis, D. C. Flanders, and H. I. Smith, Appl. Phys. Lett. 35, 71 (1970).

13. P. Nath and K. L. Chopra, Phys. Rev. B 10, 3412 (1974).

14. R. B. Gold, J. F. Gibbons, T. J. Magee, J. Peng, R. Ormond, V. R. Deline, and C. A. Evans, Jr., in Ref. 7, p. 221.

15. G. H. Gilmer and H. J. Leamy, in Ref. 7, p. 227.

16. H. J. Leamy, W. L. Brown, G. K. Celler, G. Foti, G. H. Gilmer, and J. C. C. Fan, Appl. Phys. Lett. (to be published).

17. See for example, B. Chalmers, Principles of Solidification (Wiley, New York, 1964).

18. M. Larsen, H. J. Zeiger, and B. J. Palm, Appl. Phys. Commun. (to be published).

19. R. P. Gale, J. C. C. Fan, R. L. Chapman, and H. J. Zeiger, Proceedings of the Materials Research Society Conference, Boston, MA, 1980 (to be published).

APPENDIX A - Numerical Solution of Integral Equation

The non-linear integral equation (3) cannot in general be solved exactly, and approximate solutions must be obtained numerically. Although the results are not entirely satisfactory, to solve Eq. (3) we have used a slightly modified rectangular rule to evaluate the integral, making use of the already determined values of $S(\tau')$ at earlier times τ' to evaluate $S(\tau)$ self-consistently at time τ. The modification of the rule consists of removing the singularity in the integrand at $\tau' = \tau$ by treating all terms except $(\tau-\tau')^{1/2}$ in the integrand as constant in an interval $\delta\tau'$, and integrating $(\tau-\tau')^{1/2}$ over the interval $\delta\tau'$. The integral equation (3) is then replaced by the approximate equation,

$$1 = \alpha \exp\left\{-S_n^2\right\} + n \sum_{m=0}^{n-1} \gamma_{nm} \frac{\left[\dot{S}_m + V\right]}{(\tau_n - \tau_m)^{1/2}} \exp\left\{-\Gamma(\tau_n - \tau_m)\right\} \times \qquad \text{(A1)}$$

$$\exp\left\{-\left[S_n - S_m + V(\tau_n - \tau_m)\right]^2 / (\tau_n - \tau_m)\right\} \delta\tau ,$$

where $\gamma_{nm} \equiv 2(n-m)^{1/2}\left[(n-m)^{1/2} - (n-m-1)^{1/2}\right]$, and

$\dot{S}_m \equiv \dfrac{S_m - S_{m-1}}{\delta\tau}$, $m \neq 0$; $\dot{S}_0 \equiv 0$.

S_m is the value of S at $\tau = \tau_m$, and (A1) is solved for S_n using the values of S_m determined for earlier times. When $\dot{S}_m < -V$, the assumption is made that the front has ceased to move, and $(\dot{S}_m + V)$ is set equal to zero.

Once the set of values $S_0, S_1, \ldots S_m$ has been determined, the reduced temperature at point S' at time $\tau = \tau_n$, given by Eq. (5), can be determined numerically using an approximate trapezoidal rule which yields the relation,

$$T'_n(S', \tau_n) = \alpha \exp\{-S'^2\} + \eta \sum_{m=0}^{n-1} \gamma_{nm} \frac{\left[S_m + V\right]}{(\tau_n - \tau_m)^{1/2}} \times \exp\{-\Gamma(\tau_n - \tau_m)\} \times \exp\left\{-\left[S' - S_m + V(\tau_n - \tau_m)\right]^2 / (\tau_n - \tau_m)\right\} \delta\tau \,. \quad \text{(A2)}$$

Equation (A2) has the advantage that it gives reasonable results for S' well away from S_n, and agrees exactly with (A1) for $S' = S_n$. However, it gives rise to a spurious spike near $S' = S_n$. The origin of this spike can be seen by comparing the second exponential in the integrand of Eq. (5) with the corresponding exponential in the summation of (A2). For $S' \neq S$ in Eq. (5), the exponential term $\to -\infty$ as $\tau' \to \tau$ yielding a vanishing contribution to the

integral. The term corresponding to $\tau' \to \tau$ in (A2) is

$$\frac{-[S' - S_{n-1} + V\,\delta\tau]^2}{(\delta\tau)}$$

, yielding a non-vanishing contribution of the summation which peaks up when $S' \sim S_{n-1} - V\delta\tau$ and gives rise to a spike of width $\Delta S' \sim (\delta\tau)^{1/2}$. The spikes have been substracted out in the plots of $T'(S', \tau)$ vs S' shown in Figs 7, 8, and 9.

Appendix B - Two-Dimensional Stationary Solution of a-c Boundary Problem

We consider a two-dimensional heat flow problem in which a moving source of heat scans at a steady velocity v along the surface of a film (1) of thickness b_1 deposited on a substrate (2) of thickness b_2 (see Fig. B1). If the properties of the film are the same whether it is in the crystalline or the amorphous state, we need not at the moment specify the state of the film. We assume that the moving source deposits heat only in the film and uniformly in the x-direction. The heat flow equations in regions (1) and (2) are then,

$$K_1 \left[\frac{\partial^2 T_1}{\partial x^2} + \frac{\partial^2 T_1}{\partial y^2}\right] - C_1 \rho_1 \frac{\partial T_1}{\partial t} + G\,(y-vt) = 0$$

$$K_2 \left[\frac{\partial^2 T_2}{\partial x^2} + \frac{\partial^2 T_2}{\partial y^2}\right] - C_2 \rho_2 \frac{\partial T_2}{\partial t} = 0\,,$$

where G(y-vt) is the heat energy delivered to the film per cm^3 per second.

If we consider only stationary solutions in a frame of reference moving with velocity v, then T_1 and T_2 are dependent on time only by virtue of their dependence on (y - vt). In this moving frame of reference these equations become,

$$\frac{\partial^2 T_1}{\partial x^2} + \frac{\partial^2 T_1}{\partial u^2} + \frac{C_1 \rho_1 v}{K_1} \frac{\partial T_1}{\partial u} + \frac{G(u)}{K_1} = 0 \qquad \text{(B1)}$$

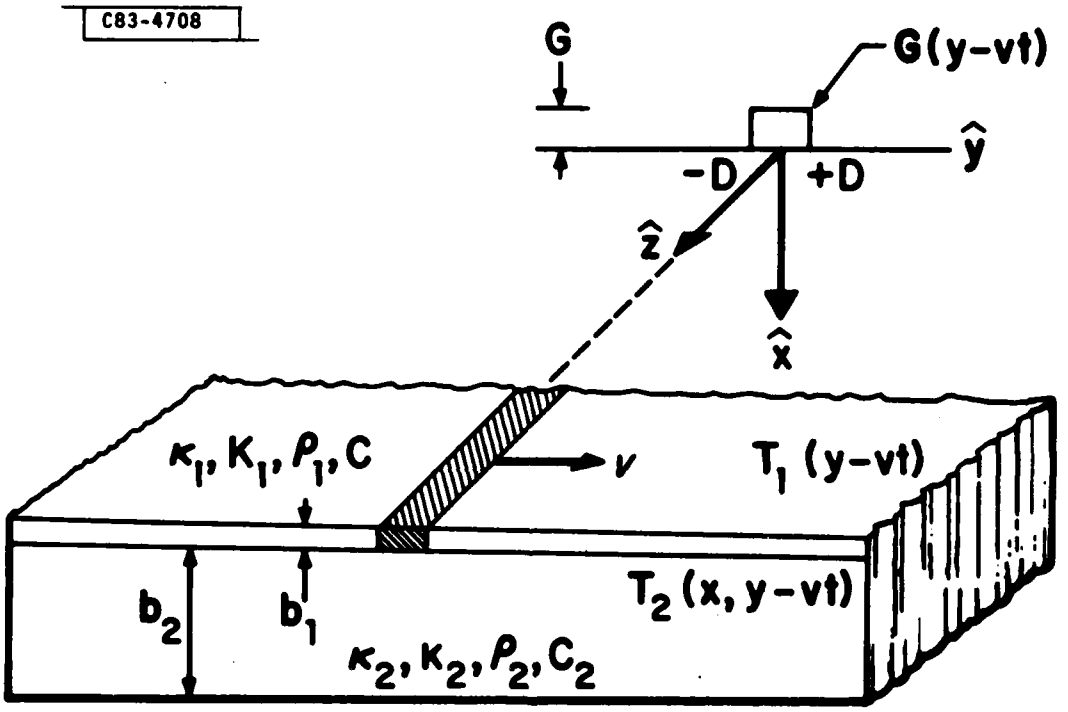

Fig. B-1. Diagram for the calculation of the exact stationary solution of moving a-c boundary problem.

$$\frac{\partial^2 T_2}{\partial x^2} + \frac{\partial^2 T_2}{\partial u^2} + \frac{C_2 \rho_2 v}{K_2} \frac{\partial T_2}{\partial u} = 0 \qquad \text{(B2)}$$

where $u = y - vt$.

The heat flow out of the film surface is zero:

$$\left[\frac{\partial T_1(x,u)}{\partial x}\right]_{x=0} = 0 \qquad \text{(B3)}$$

The boundary conditions at the interface between film and substrate require that the temperature and heat flow across the boundary are continuous:

$$[T_1(x,u)]_{x=b_1} = [T_2(x,u)]_{x=b_1} , \qquad \text{(B4)}$$

$$K_1 \left[\frac{\partial T_1(x,u)}{\partial x}\right]_{x=b_1} = K_2 \left[\frac{\partial T_2(x,u)}{\partial x}\right]_{x=b_1} . \qquad \text{(B5)}$$

At the base of the substrate the temperature is T_b:

$$[T_2(x,u)]_{x=(b_1 + b_2)} = T_b . \qquad \text{(B6)}$$

We now assume the film is so thin that the temperature variation across it is quite small. Integrating (B1) with respect to x, and using (B3) and

(B5) to eliminate $\partial T_1/\partial x$ yields,

$$\frac{K_2}{b_1 K_1}\left[\frac{\partial T_2}{\partial x}\right]_{x=b_1} + \frac{\partial^2 T_1}{\partial u^2} + \frac{\rho_1 C_1 v}{K_1}\frac{\partial T_1}{\partial u} + \frac{G(u)}{K_1} = 0 \qquad (B7)$$

Finally, if we allow b_1 to become very small compared to b_2, we can write the coupled equations to be solved for $T_1(u)$ and $T_2(x,u)$ as,

$$\frac{\partial^2 T_2}{\partial x^2} + \frac{\partial^2 T_2}{\partial u^2} + \frac{v}{\kappa_2}\frac{\partial T_2}{\partial u} = 0 \qquad (B8)$$

$$\frac{K_2}{b_1 K_1}\left[\frac{\partial T_2}{\partial x}\right]_{x=0} + \frac{\partial^2 T_1}{\partial u^2} + \frac{v}{\kappa_1}\frac{\partial T_1}{\partial u} + \frac{G(u)}{K_1} = 0 \qquad (B9)$$

with boundary conditions

$$T_1(u) = [T_2(x,u)]_{x=0} \qquad (B10)$$

$$[T_2(x,u)]_{x=b_2} = T_b \ . \qquad (B11)$$

We introduce the Fourier integrals of $(T_1(u)-T_b)$ and $(T_2(x,u) - T_b)$:

$$\tau_1(k) = \int_{-\infty}^{\infty} (T_1(u) - T_b)\, e^{iku}\, du \qquad (B12)$$

$$\tau_2(x,k) = \int_{-\infty}^{\infty} (T_2(x,u) - T_b) e^{iku}\, du \ , \qquad (B13)$$

with inverses

$$T_1(u)-T_b = \frac{1}{2\pi} \int_{-\infty}^{\infty} \tau_1(k)\, e^{-iku}\, dk \ , \tag{B14}$$

$$T_2(x,u)-T_b = \frac{1}{2\pi} \int_{-\infty}^{\infty} \tau_2(x,k)\, e^{-iku}\, dk \ . \tag{B15}$$

Applying (B12) - (B15) to (B8) - (B11), we obtain

$$\frac{\partial \tau_2}{\partial x^2} - \alpha_2^2\, \tau_2 = 0 \tag{B16}$$

$$\frac{K_2}{b_1 K_1} \left[\frac{\partial \tau_2}{\partial x}\right]_o - \alpha_1^2\, \tau_1 + \frac{g}{K_1} = 0 \tag{B17}$$

$$\tau_1 = [\tau_2]_o \tag{B18}$$

$$[\tau_2]_{b_2} = 0 \tag{B19}$$

where $g(k)$ is the Fourier transform of $G(u)$,

$$g(k) = \int_{-\infty}^{\infty} G(u)\, e^{iku}\, du \ , \tag{B20}$$

$$\alpha_2^2 = k^2 + i\, \frac{vk}{\kappa_2} \ , \text{ and}$$

$$\alpha_1^2 = k^2 + i\, \frac{vk}{\kappa_1} \ .$$

The solution of (B16) is of the form,

$$\tau_2 = Ae^{\alpha_2 x} + Be^{-\alpha_2 x} \quad . \tag{B21}$$

Substitution of (B21) into (B18) and (B19) permits the expression of A and B in terms of τ_1. Further substitution of these expressions into (B17) gives the solution for τ_1 in the form,

$$\tau_1 = \frac{g/K_1}{\alpha_1^2 + \alpha_2 \frac{K_2}{b_1 K_1} \coth(\alpha_2 b_2)} \tag{B22}$$

The inverse Fourier transform (B14) leads to the result,

$$T_1(u) = T_b + \frac{1}{2\pi} \int_{-\infty}^{\infty} \frac{g(k)/K_1 \, e^{-iku} \, dk}{\alpha_1^2 + \alpha_2 \frac{K_2}{b_1 K_1} \coth(\alpha_2 b_2)} \quad . \tag{B23}$$

We will take $G(y-vt) = G(u)$ to be of the form,

$$G(y-vt) = G \cdot \theta(u) \text{ where } \theta(u) = 0,\ u < -D,\ u > D, \tag{B24}$$
$$\theta(u) = 1,\ -D < u < D \ .$$

This form yields,

$$g(k) = \frac{2 \sin kD \cdot G}{k} \quad . \tag{B25}$$

It is important to note that for several heat sources, g(k) is the superposition of contributions due to the individual sources. Thus, for a case in which separate laser and latent heat inputs are present, the solution of the problem is the sum of individual terms of the form (B23).

With g(k) taken to be of the form (B25), we will write the integral (B23) in terms of normalized quantities. We introduce a characteristic normalization length d to be specified and write,

$$T_1(S') = T_b + \frac{1}{2\pi} p\int_{-\infty}^{\infty} \frac{(Gd^2/K_1)\ 2\ \sin qD'}{q} \quad \frac{e^{-iqS'}\, dq}{-4\Gamma(q) + \beta Q(q)\ \cot\ Q(q)} \qquad \text{(B26)}$$

where $q = kd$, $D' = D/d$, $S' = u/d$,

$$2i\,\Gamma(q)^{1/2} = \alpha_1 d = [q^2 + 4iVq]^{1/2},$$

$$Q(q) = -i(\alpha_2 d)\ (b_2/d) = 2\ [\Gamma + 2V\ \{M-1\}\ \{-V \pm [\Gamma + V^2]^{1/2}\}]^{1/2}\ (b_2/d), \qquad \text{(B26a)}$$

and

$$\beta = \frac{K_2 d^2}{K_1 b_1 b_2} \quad ,$$

$$M = \kappa_1/\kappa_2 \quad ,$$

$$V = dv/4\kappa_1 \quad .$$

The quantities β,M,V are the important parameters of the model. For convenience we will in this appendix, choose $d = b_2$ so that β becomes

K_2b_2/K_1b_1. The ($\pm$) sign in $Q(q)$ represents the fact that for a given value of $\Gamma(q)$, there are two values of q given by,

$$q = 2i \{-V \pm [\Gamma + V^2]^{1/2}\}$$

with the + sign corresponding to postive imaginary q and the minus sign corresponding to negative imaginary q.

The notation $p \int_{-\infty}^{\infty}$ signifies the principal part of the integral:

$p \int_{-\infty}^{\infty} dq = \int_{-\infty}^{-\varepsilon} dq + \int_{+\varepsilon}^{\infty} dq$, where ε is an infinitesimal quantity. This is important in evaluating (B26), since the integral is singular at $q = 0$.

The integrand in (B26) is a single-valued function of q with poles given by $q = 0$ and

$$D(q) = -4\ \Gamma(q) + \beta Q(q) \cot Q(q) = 0 \quad . \tag{B26b}$$

If $Q(q)$ is complex, as it will be for much of the complex q-plane, $Q(q) \cot Q(q)$ is still well defined. For $Q(q)$ pure imaginary, $Q\cot Q \to |Q| \coth |Q|$.

The integral can be evaluated by contour integration after appropriately closing contours at $|q| = \infty$. Sin qD' is written as $(e^{iqD'} - e^{-iqD'})/2i$, and the individual integrals are of the form

$$p \int_{-\infty}^{\infty} e^{-iqZ} f(q)\, dq \quad .$$

For $Z > 0$, the contour is closed in the lower half plane, while for $Z < 0$, the

contour is closed in the upper half plane. The integrals can be evaluated using the residue theorem. The contributions from the zeros of D(q) are obtained by writing D(q) in the vicinity of the n-th pole as

$$D(q)_n \cong \left[\frac{\partial D(q)}{\partial q}\right]_{q = q_n} (q - q_n) \quad ,$$

which introduces a factor of $(\partial D(q)/\partial q)_{q=q_n}$ into the denominator of the expression for the n-th residue. For large values of the parameters β, the case of interest here, the zeros of D(q) lie on the imaginary q axis in both the upper and lower half plane (corresponding to $\Gamma(q)$ real).

Without going through all of the arithmetic, we present the results of the evaluation of (B26) after performing the contour integrations. $T_1(S')$ can be written as,

$$T_1(S') = T_b + \sum_{n+} (Gd^2/K_1) \{F_{n+}(S' - D') - F_{n+}(S'+D')\} \qquad (S' < -D')$$

$$T_1(S') = T_b + \sum_{n+} (Gd^2/K_1) F_{n+}(S' - D') \qquad \text{(B27)}$$

$$- \sum_{n-} (Gd^2/K_1) F_{n-}(S' + D') + \frac{(Gd^2/K_1)}{\beta} \qquad (-D' < S' < D')$$

$$T_1(S') = T_b + \sum_{n-} (Gd^2/K_1) \{F_{n-}(S' + D') - Fn -(S' - D')\} \qquad (D' < S')$$

where

$$F_{n\pm}(Z) = \frac{e[-V \pm (\Gamma_{n\pm} + V^2)^{1/2}]2Z}{(\partial D_{\pm}/\partial\Gamma)_{n\pm}(\partial\Gamma/\partial q)_{n\pm} 2i[-V \pm (\Gamma_{n\pm} + V^2)^{1/2}]} \quad , \tag{B28}$$

$$D_{\pm} = -4\Gamma(q) + \beta Q_{\pm}(q) \cot Q_{\pm}(q) \quad ,$$

$$-4\Gamma(q) = q^2 + 4\, iVq, \text{ and}$$

$$Q_{\pm}(q) = 2[\Gamma + 2V[M - 1]\{-V \pm (\Gamma + V^2)^{1/2}\}]^{1/2}.$$

The $\Gamma_{n\pm}$ correspond to the zeros of $D_{\pm}$. The values of q corresponding to $\Gamma_{n\pm}$ are

$$q_{n\pm} = 2\, i\, \{-V \pm [\Gamma_{n\pm} + V^2]^{1/2}\} \quad .$$

The Γ's are real numbers while the q's lie along the imaginary axis.

We will be concerned with the case where D' is very small. Expanding $F_{n\pm}(S' - D')$ and $F_{n\pm}(S' + D')$ to first order in D', and taking the remaining derivatives in (B28), we obtain

$$T_1(S') = T_b + \sum_{n+} \frac{D'(Gd^2/K_1)}{[2 - \beta\left\{\frac{\cot Q_{n+}}{Q_{n+}} - \csc^2 Q_{n+}\right\}\left\{1 + \frac{V(M-1)}{\sqrt{(\Gamma_{n+} + V^2)}}\right\}]} \times$$

$$\frac{e^{-2VS'}\, e^{-2\,[r_{n+} + V^2]^{1/2}\,|S'|}}{[r_{n+} + V^2]^{1/2}} \qquad (S' < 0)\ ,$$

$$T_1(S') = T_b + \sum_{n^-} \frac{D'\,(Gd^2/K_1)}{\left[2 - \beta\left\{\frac{\cot Q_{n-}}{Q_{n-}} - \csc^2 Q_{n-}\right\}\left\{1 - \frac{V\,(M-1)}{\sqrt{(r_{n-} + V^2)}}\right\}\right]} \times$$

$$\frac{e^{-2VS'}\, e^{-2\,[r_{n-} + V^2]^{1/2}\,|S'|}}{[r_{n-} + V^2]^{1/2}} \qquad (B29)$$

$$(S' > 0).$$

Now, suppose that the source of heat energy delivered to the film is the latent heat given up as the a-c boundary moves. The energy G delivered per cm^3 per second is,

$$G = \frac{L\rho_1 v}{2D}\ ,$$

where 2D is the width of the region over which this energy is delivered in

time 2D/v. Introducing normalized quantities,

$$(Gd^2/K_1) = \frac{2\,L\,V}{C_1\,D'} \quad . \tag{B30}$$

Substitution of (B30) into (B29) and some simple manipulation of the resulting expression leads to,

$$T_1(S') = T_b + \frac{LV}{C_1} \sum_{n+} \frac{e^{-2VS'}\, e^{-2[r_{n+} + V^2]^{1/2}\,|S'|}}{[r_{n+} + V^2]^{1/2}} \quad x \tag{B31a}$$

$$\frac{1}{[1-\beta/2 \left\{\frac{\cot Q_{n+}}{Q_{n+}} - \csc^2 Q_{n+}\right\} \left\{1 + \frac{V(M-1)}{\sqrt{(r_{n+} + V^2)}}\right\}]}$$

$$(S' < 0) \quad ,$$

$$T_1(S') = T_b + \frac{LV}{C_1} \sum_{n-} \frac{e^{-2VS'}\, e^{-2[r_{n-} + V^2]^{1/2}\,|S'|}}{[r_{n-} + V^2]^{1/2}} \quad x \tag{B31b}$$

$$\frac{1}{\left[1 - \beta/2 \left\{\frac{\cot Q_{n-}}{Q_{n-}} - \csc^2 Q_{n-}\right\} \left\{1 - \frac{V(M-1)}{\sqrt{(\Gamma_{n-} + V^2)}}\right\}\right]}$$

$(S' > 0)$.

Equations (B31a)and (B31b) are used to calculate the velocity of the a-c boundary in the steady-state runaway condition in Sec IIIB.

(14) TR-558

UNCLASSIFIED

SECURITY CLASSIFICATION OF THIS PAGE *(When Data Entered)*

(19) **REPORT DOCUMENTATION PAGE**

READ INSTRUCTIONS BEFORE COMPLETING FORM

1. REPORT NUMBER (18) ESD-TR-81-85	2. GOVT ACCESSION NO. AD-A105811
3. RECIPIENT'S CATALOG NUMBER	
4. TITLE *(and Subtitle)* (6) Amorphous-Crystalline Boundary Dynamics in Laser Crystallization	5. TYPE OF REPORT & PERIOD COVERED (9) Technical Report
	6. PERFORMING ORG. REPORT NUMBER Technical Report 558
7. AUTHOR(s) (10) Herbert J. Zeiger, John Chin C. Fan, Barbara J. Palm, Ralph L. Chapman and Ronald P. Gale	8. CONTRACT OR GRANT NUMBER(s) (15) F19628-80-C-0002
9. PERFORMING ORGANIZATION NAME AND ADDRESS Lincoln Laboratory, M.I.T. P.O. Box 73 Lexington, MA 02173	10. PROGRAM ELEMENT, PROJECT, TASK AREA & WORK UNIT NUMBERS (16) Program Element No. 63250F Project No. 6491
11. CONTROLLING OFFICE NAME AND ADDRESS Air Force Systems Command, USAF Andrews AFB Washington, DC 20331	12. REPORT DATE (11) 25 August 1981
	13. NUMBER OF PAGES (12) 76
14. MONITORING AGENCY NAME & ADDRESS *(if different from Controlling Office)* Electronic Systems Division Hanscom AFB Bedford, MA 01731	15. SECURITY CLASS. *(of this report)* Unclassified
	15a. DECLASSIFICATION DOWNGRADING SCHEDULE

16. DISTRIBUTION STATEMENT *(of this Report)*

Approved for public release; distribution unlimited.

17. DISTRIBUTION STATEMENT *(of the abstract entered in Block 20, if different from Report)*

18. SUPPLEMENTARY NOTES

None

19. KEY WORDS *(Continue on reverse side if necessary and identify by block number)*

amorphous-crystalline boundary dynamics
thin film microstructure
solid-liquid transformation
solid-solid transformation

20. ABSTRACT *(Continue on reverse side if necessary and identify by block number)*

Two theoretical descriptions of phase boundary dynamics during cw laser crystallization of thin amorphous semiconductor films have been developed. The first reduces the problem to the solution of a one-dimensional integral equation, yielding a semi-empirical fit of the spatial periodicity observed in crystallized films as a function of background temperature. The model qualitatively explains many of the effects observed during laser crystallization, including periodic fluctuations in light emission. The second theoretical description is a two-dimensional heat flow calculation applicable only to the case of steady-state boundary motion. This model, which contains no ad hoc parameters, yields boundary velocities for thin films of Ge on fused silica which fall in the range 100-300 cm/sec observed experimentally.

DD FORM 1 JAN 73 1473 EDITION OF 1 NOV 65 IS OBSOLETE

UNCLASSIFIED

SECURITY CLASSIFICATION OF THIS PAGE *(When Data Entered)*

207650

JOB

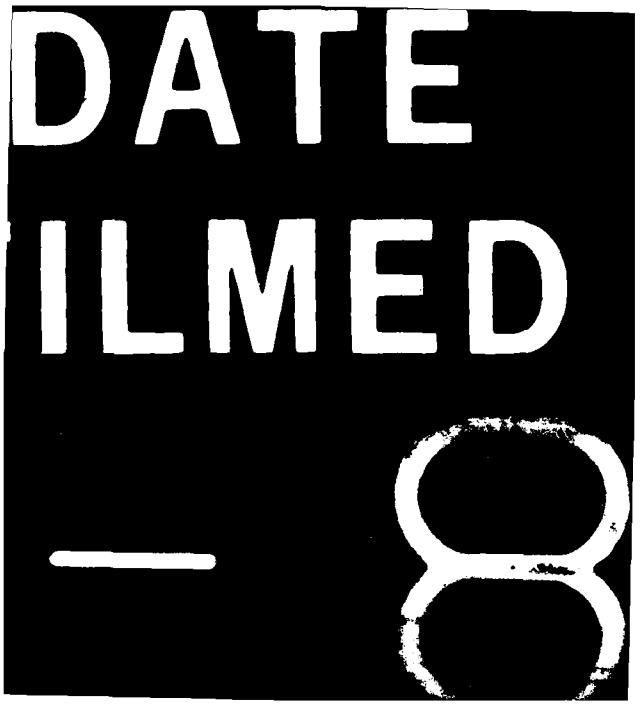
DATE
ILMED
8